Crack Detection in Aluminum Structures

by
Brad A. Butrym

Thesis submitted to the faculty of the Virginia Polytechnic Institute and State University in partial fulfillment of the requirements for the degree of

Master of Science
In
Mechanical Engineering

Daniel J. Inman
Mary E. Kasarda
Myung-Hyun Kim

April 26, 2010
Blacksburg Virginia

Keywords: Structural Health Monitoring, Stress Intensity Factors, Macro Fiber Composite, Piezoelectric, NDE.

Crack Detection in Aluminum Structures

Brad A. Butrym

ABSTRACT

Structural health monitoring (SHM) is the process of using measurements of a structure's response to known excitations and trying to determine if damage has occurred to the structure. This also fits the description of non-destructive evaluation (NDE). The main difference is that NDE takes place while the structure is out of service and SHM is intended to take place while the structure is in service. As such, SHM provides the opportunity to provide early warning against structural failure. This thesis intends to advance the state of the art in SHM by examining two approaches to SHM: vibration based and impedance based, and to associate these with the NDE method of stress intensity factors. By examining these methods the goal is to try and answer some of the important questions in SHM process. The first is to experimentally validate a crack model and to see how small of a crack can be detected by vibration methods. The second is to use the concept of stress intensity factor to perform an SHM type of measurement to determine the remaining life of a structure once the impedance method has determined that damage has occurred.

The measurement system considered consists of using several different piezoceramic materials as self-sensing actuators and sensors. The structures are a simple beam and a more complex lug element used in aircraft applications. The approach suggested here is to use the impedance and vibration methods to detect crack initiation and then to use the proposed stress intensity method to measure the stress intensity factor of the structure under consideration.

Acknowledgements

I would like to acknowledge my advisor Dr. Inman for all of his guidance and support throughout this process. I would also like to thank my colleagues at CIMSS for all of your help and input, especially Alper Erturk for serving as a proxy on my thesis defense committee. Finally I would like to thank my wonderful girlfriend Krissy Shahade for all of her love and support.

All photographs contained in this thesis are by Brad Butrym, 2010.

Table of Contents

List of Tables:

List of Figures:

List of Variables

A	Cross sectional area of Euler-Bernoulli Beam
a_i	Crack depth
C	Geometry constant for calculation of analytical Stress intensity factor
Ci	Compliance of the beam at the crack location
dv/dx	Slope of differential element
E	Modulus of Elasticity
H	Beam height
H_0	Distance from active area of MFC to crack propagation path for SIF experiment
I	Area moment of Inertia
k	Stress state constant
Ki	Mode 1 stress intensity factor
Kii	Mode 2 stress intensity factor
L	Beam Length
$L1$	Geometry constant from SIF experiment
$L2$	Geometry constant from SIF experiment
$M(0)$	Moment at fixed end of beam
P	Static Axial Force
$Re(Z_{i,j})$	Real impedance measurement j point i
S	Active Surface area of MFC
V	Transverse displacement
V	Peak to peak voltage output of MFC for SIF experiment
$V(0)$	Shear Force at Fixed end of beam
W	beam width
$X(0)$	Displacement at fixed end of beam
$X(x)$	Mode Shape
Xc	Crack Distance from origin
B	Constant used to calculate natural frequency of cantilever beam
ρ	Mass Density
σ	Stress range
$\varphi(0)$	Rotation at fixed end of beam
ω	Natural Frequency

Chapter 1: Introduction and Related work

1.1 Non-Destructive Evaluation (NDE)

Non-destructive evaluation is widely used in industry to evaluate the structural integrity of civil and mechanical structures. The evaluation is performed by an NDE specialist and is generally performed on a routine maintenance schedule when the structure is out of service. Many NDE methods are available and are currently being used commercially. A good reference for NDE is Schull (2002). The difference between NDE and structural health monitoring (SHM) is that SHM is an online system that is intended to be performed while the structure is in service. NDE methods include ultrasound, thermal wave, Eddy Currents, vibration methods, surface waves, and acoustic emission. SHM methods also include vibration, wave propagation, and acoustic emission. Monitoring techniques are applied to structures such as airframes, bridges, and turbo machinery.

A vibration method for NDE of metal adhesive joints using changes in modal damping is presented in Pandurangan and Buckner (2006). An NDE method of measuring stress intensity factors using piezoelectrics is introduced in Yukio Fujimoto (2003). The stress intensity factor method will be a subject of research in this thesis. A good reference for a review of NDE technologies is given in Heyman (1990).

1.2 Structural Health Monitoring

Structural Health Monitoring (SHM) is the process of evaluating structures, continuously or periodically, while the structure is in service, in order to predict failure at an early stage. The difference between NDE and SHM is that SHM is an online system. Columns and beams are used in many machines and structures in engineering. According to Aydin (2008) cracks in these

parts can not only cause a decrease in the critical loading of the part, but can cause vibration response problems as well. Current NDE methods of inspecting structures require scheduled down time where the part is removed from service for evaluation. Structural health monitoring aims to make it possible to only remove the structural element from service when its integrity has deteriorated. Economic concerns, aging infrastructure, and media coverage of catastrophic failures have led to much research in SHM techniques. A good reference for piezoelectric based SHM is Giurgiutiu (2008). Farrar et al. (2006) provides a good overview of different sensing techniques that can be used for the data acquisition portion of SHM.

Many different methods of SHM are currently being investigated. Guided wave measurements such as Lamb waves are often employed. A good reference for Lamb wave based SHM is Anton et al. (2007). Wave propagation using piezoelectric sensors and actuators is also studied in Mi et al. (2006) and Yuhang and Yaowen (2007). Active damage interrogation is a system which uses embedded Piezo-electric patches as sensors and actuators to assess damage. The method is presented in Lichtenwalner et al. (1997), and uses broadband excitation to determine the transfer function between various actuator and sensor pairs. A cumulative average delta damage metric is used to determine the severity of the change in transfer function between the healthy case and the current case. Wavelet analysis is used to detect, locate, and quantify damage in a cantilever beam in Loutridis et al. (2004).

1.3 Piezoelectric Effect

The sensors and actuators used here are piezoelectric materials. Piezoelectrics are used due to their ability to be used as sensors and actuators as well as their ability to respond at high frequencies. Macro fiber composites as well as raw PZT-5H are the specific type of piezoelectric materials used here. PZT-5H is lead zirconate titanate. According to Leo (2007),

smart materials are classified as any material that exhibits direct coupling between two physical domains. Examples of these materials include thermo-electric, piezoelectric, and shape memory alloys (SMA). Piezoelectric materials exhibit coupling between mechanical strain and electric charge. This effect is known as electromechanical coupling. This effect is attributed to an asymmetry of charge in the crystal structure of a piezoelectric molecule. When the material is stressed, the charged particles in the material move. This motion is called "electric displacement" and will cause a net voltage which can be measured at the electrodes. The converse effect is when an electric field is applied to the material causing electric displacement and therefore producing mechanical strain (Leo, 2007). The piezoelectric effect is highly useful in a variety of applications. Piezoelectrics can be used as sensors and actuators for NDE and SHM systems.

1.4 Vibration Methods

1.4.1 Natural Frequencies as Damage Indicators

Conventional methods for NDE crack detection include visual inspection, radiography, and acoustic emission according to Aydin (2008). These methods are rather limited in the information they provide and can be inaccurate. They can only provide level one (existence of damage) and limited level two information (location of damage). Generally, conventional methods can only tell that the structure is damaged. In order to determine the location of the damage, many sensors are necessary. With vibration based methods it may be possible to acquire global damage assessment using a single sensor (Cawley (1979).Using fewer sensors is less costly in terms of initial cost and maintenance costs. Using these methods it may be possible to not only determine that the structure is damaged, but also the location and severity of the damage. Despite these apparent advantages to using natural frequencies for damage detection,

some trade-offs do exist. The problem that occurs is one of false alarm damage which is a problem that all SHM methods must take into account. Since natural frequencies can be sensitive to atmospheric conditions and temperature it may be difficult to determine whether a structure is damaged or if other conditions have affected the experimental results. A compensation technique would be required to account for atmospheric conditions.

Vibration methods study the structural or modal parameters of a structure. Structural parameters include mass, stiffness, and flexibility. Modal parameters are functions of the structural parameters and are more often used. The modal parameters include natural frequencies, modal damping, and mode shapes. According to Aydin (2008) natural frequency has been studied most often due to its relative ease of measurement. By using a vibration model it is possible to minimize the number of necessary sensors and maximize the information provided through data analysis.

Much research has been conducted in crack modeling for tracking natural frequency shifts. There are many ways of measuring natural frequency shifts. A low power method with no direct human interaction would be ideal. According to Doebling et al. (1998) natural frequencies may be poor indicators of damage. Either very large cracks or very precise measurements are necessary to detect damage with vibration based methods. Compared to other methods, much power is necessary to excite multiple vibration modes. This could mean that self-excited structures, such as airplane wings, would be more conducive to vibration based SHM techniques. Non-linear dynamics of breathing cracks may be a promising area of research for rotating machinery. Despite these drawbacks, much research has been conducted in crack modeling for natural frequency monitoring.

1.4.1.1 Natural Frequency method literature.

Many models for the natural frequencies of cracked beams have been presented over the years. The idea of monitoring natural frequencies is well developed and has been studied much over the years although it has not been widely implemented in real structures. A good review of this technology is given in Salawu (1997). Chondros and Dimarogonas (1980) used natural frequencies as damage indicators for the weld joints at the base of cantilever beams. Natural frequencies are used to detect multiple cracks in a beam in Khiem and Lien (2004). Crack localization in beams is achieved using relative amplitudes of modal frequencies in Narkis (1994). Some of the challenges associated with applying this technology to civil structures have been presented in Duan et al. (2008). In Zhang (1999) it is found that damping values as well as natural frequencies are significantly affected by the non-linear effect of the opening and closure of fatigue cracks in structural members.

1.4.1.2 Inherently non-linear behavior of breathing cracks

Non-linear phenomenon in the measurement of natural frequencies is also an extensive area of research. A review of the non-linear dynamics of complex structures is given in Brandon (2000). The idea is presented that research to this point has been too academic. Only limited work has been done on finding robust indicators of damage induced non-linearity in signals that can be used by designers. One property of a non-linear system is that the system will respond at frequencies outside of the excitation spectrum. The non-linearity of breathing cracks was idealized as a bilinear stiffness by Chondros et al. (1998). It was found that super harmonics in the Fourier spectrum can be correlated to this bilinear behavior. According to Doebling, Farrar et al. (1998), non-linear behavior is easier to detect than frequency changes. Detecting non-linear behavior could also be used to detect damage without the need for a model. This is a

promising area of research for Rotordynamics, however, for SHM of structural members in remote locations the computational cost of detecting non-linearity may be restrictive.

1.4.2 Beat Phenomenon

A method of damage detection using beat frequencies has been proposed in Cattarius (1997) and Cattarius (2000). In these papers time series data recorded from piezoelectric sensors is used to detect faults in rotor blades. The measurements are free decay signals. Free decay signals are generated when a structure is excited near resonance and the excitation is turned off. The signal that results as the vibration decays is known as a free decay signal. When two free decay vibration response signals are very close in frequency, the subtraction of one signal from the other will result in beating in time. When a structure is cracked the natural frequencies will shift. The frequency of free decay signals will be used to visualize this shift. The beating phenomena will be helpful to visualize small differences in frequency that may be undetectable by other frequency shift methods. The fact that time domain signals are used is also advantageous as it avoids error introduced through the use of Fourier transform methods. Carneiro (2000) developed a time domain method for identification of crack location and depth in order to avoid the data loss associated with frequency domain methods. By using the beat method it is hoped that smaller shifts in natural frequencies, and therefore less severe damage than the natural frequency method, can be detected. This method will also be capable of monitoring the natural frequency to provide additional information to our damage detection algorithm. This is done by taking the Fourier transform of the free decay signals which will result in the frequency response function for the test specimen at different levels of cracking.

1.5 Impedance

The Impedance method is a well known approach to structural health monitoring (Grisso and Inman (2006)). An overview of the impedance method is given in Park et al. (2003). The impedance method uses a piezoelectric wafer as a self sensing actuator. The method is based on the phenomena of electrical impedance of a PZT being directly related to the mechanical impedance of the host structure as is outlined in Liang et al. (1994). Although a model for piezoelectrics bonded to real structures is not considered, a model for the relationship between impedance of piezoelectric materials and their host structures is given in Liang et al. (1996). One of the advantages of the impedance method used here is that it is not model based. This means that baseline measurements are necessary; however, the method is very applicable to real structures which can be difficult to model. The drawback of not having a model is that the information this method provides is somewhat limited. The method is very suitable to determining that damage has occurred, or has increased in severity, but is not suited to quantifying damage. This is a very promising field for SHM due to the ability to detect early stage cracks. The development of a small form factor, low power, and low cost impedance analyzer would be advantageous in the application of this technology to real world structures. A chip based impedance analyzing system is developed and studied in Park et al. (2007) for detecting corrosion on aluminum beams using macro fiber composites.

Impedance of piezoelectrics has been studied widely in the literature. The impedance method is used to detect pitting and delaminating of wind turbine blades in Pitchford (2007). Grisso and Inman (2006) used the impedance method to detect various types of damage in thermal protection systems. Temperature can cause a lateral shift in the peaks of the impedance signatures. A compensation technique to account for this shifting is presented in Koo et al.

(2007) which uses an algorithm that shifts the spectrum so that maximum correlation between the signals is found. This can be used to effectively cancel out the effect of temperature on the impedance signatures.

1.6 Stress Intensity factors

The fatigue life of a structure is defined as the sum of the crack initiation life and the crack propagation life. The crack initiation life is the number of cycles necessary to induce a fatigue crack. The crack propagation life is the number of cycles required to induce failure when final fracture occurs. Cracks will occur at the area of greatest stress in a part, called "hotspots", therefore it is possible to know the locations where cracks will initiate in structures if the stress distribution is known.

Stress Intensity Factors (SIF) are used in linear elastic fracture mechanics to describe the stress state near the crack tip. They are useful for providing failure criteria for materials in the presence of a crack. The stress concentration factor is defined as the ratio of maximum stress to nominal stress. Similarly the stress intensity factor is a parameter that describes the stress state in the vicinity of a crack tip considering the sample geometry, the size and location of the crack, and the magnitude of loads on the material. When stress intensity factor is above the critical SIF value, also known as fracture toughness, crack propagation occurs.

Cracks typically grow until they reach a critical size. Stress intensity factors can give us an idea of whether the stresses in a part will cause cracks to propagate. While analytical expressions for SIF for simple geometries exist, it has become increasingly difficult and more computationally expensive to predict theoretical stress intensity factors. This is due to the complexity of modern structures. The calculations, in particular, become expensive when weld joints, complex loads, and complex geometries come into play. Weld joints are one of the most critical areas in many

real structures. Finite element procedures can be used for analysis in many cases but can sometimes provide inaccurate results due to insufficient material data. The modeling could be avoided if a robust and inexpensive way of measuring SIFs on real structures is developed. This would be especially useful if it could be accomplished on weld joints.

This analysis follows the method of Fujimoto (2004) to relate the measured voltage output of macro-fiber composite patches (MFC) to the stress intensity factor due to a fatigue crack. The algorithm for relating voltage to stress intensity factors is given in chapter 3.

Some of the literature pertaining to SIF measurements is briefly reviewed in this section. An alternate method of measuring SIF using thermo-elasticity is discussed in F. A. Diaz (2004). In Mitsura Egashira (1993) local strain was measured using piezoelectric polymers. By relating voltage output of the piezoelectric to strain, the Egashira research set the stage for the later development of SIF measurement using Piezo-electric polymers. Finally in Yukio Fujimoto (2003) a method of measuring the SIF of a cracked structural member was developed. The voltage output of piezoelectric elements is related to the stress field at the crack tip and is then used to accurately predict the SIF of the structure. Ashby (1999) presents an analytical solution for stress intensity factors of simple geometries based on the stress range and crack length.

1.7 Thesis Contributions

This manuscript advances the state of the art in the following ways. First, multiple SHM methods are performed on a similarly sized beam so a direct comparison can be drawn between them. This will be useful in helping to determine the various SHM methods that will be applicable in different situations. It has been proposed that structural loading conditions can cause false positives in the impedance method. In this analysis the impedance method is examined when the specimen is under a static load as well as under sinusoidal axial loading. In

both conditions cracks were detected at a similar size. From this it has been concluded that the impedance method is useful for in service applications when the specimen is under a sinusoidal loading scheme. Vibration and Impedance experiments are conducted using two types of saw cut. One beam is cut in the same plane as the plane of actuation of the piezoelectric. The other is cut in a plane perpendicular to actuation. It was found that the vibration method is capable of detecting "In Plane" damage at a smaller size than out of plane damage. However, when the percentage of material that is removed is considered, the crack is detectable at similar percentages. The impedance method is capable of detecting both types of damage, however, it can detect the in plane damage more robustly. Finally, the method of measuring stress intensity factors has been validated and improved for fatigue cracks in beams. The limits of a surface integration in the algorithm previously presented were inaccurate when used on our specific geometry. By altering these limits to account for the changing stress field as the crack grows we were able to greatly improve the accuracy of the algorithm.

Chapter 2: Modeling

2.1 Crack Modeling in Simple Structures

Many models have been presented to describe the behavior of cracked beams. According to Friswell (2002), crack models can be categorized as localized reductions in stiffness, discrete spring models and finite element models in two or three dimensions. Localized reductions in stiffness have been studied by Binici (2005). Finite element models of cracks have been researched by Abdul-Aziz et al. (2006). In this thesis, a simplified model for a single crack in a long slender beam is evaluated to find the smallest detectable crack using the stiffness reduction method. It is assumed that it is possible to measure modal frequencies to within half of a hertz. It would be ideal to have a simple model that describes the physical system well and can detect early stage cracks before they start to grow.

The subject of the natural frequency study presented here is to quantify the smallest crack detectable in a cantilever Euler-Bernoulli beam compared to detectable crack size using the beat method as well as the impedance method. In order for applications of natural frequency based SHM methods to be useful, it is important to determine how sensitive natural frequencies are to crack propagation. Since fatigue cracks are a very common type of damage it would be especially useful to be able to detect this mode of crack using natural frequencies.

2.2 Euler Bernoulli Beam Theory with Cracks

The single-cracked beam in this analysis is assumed to be a combination of two sections of beam connected by a mass-less spring. The geometry is shown in figure 2.2.1. The model presented in this report was introduced by Aydin (2008) and is a variation of a model from Khiem and Lien (2001). The model presents a second order determinant in order to establish the frequency

equation. The natural frequency is a function of the geometry of the beam, support conditions, axial loading, crack location, and crack severity. The model is for beams of uniform cross sectional area and the cracks are considered to be non-breathing. This means that the crack remains open during deformation. The breathing of cracks is an extensive area of research because breathing cracks introduce nonlinearity to the system. Here we only treat the linear case.

The beam analyzed has cantilever boundary conditions. The model is capable of handling other boundary conditions as well. The crack model used is based on the strain energy function and is described more thoroughly in Dimarogonas (1996). The method presented here treats a crack as a localized reduction in stiffness and models this as a mass-less rotational spring at the location of the crack. The beam is then considered to be of multiple sections connected by springs. For the cantilever configuration the crack should be located close to the fixed end of the beam for highest sensitivity. According to Aydin (2008), the fundamental frequency of the cantilever beam will be the most sensitive to damage.

The equation of motion for Euler-Bernoulli beams can be found through a force balance on the differential element of the beam. Here, I denotes the area moment of inertia of the cross section, E is the modulus of elasticity of the material and dv/dx is the slope of the differential element. The static axial force is represented by P. The distance of the crack from the origin is X_c. From a force balance the equation of motion for transverse vibration is established. The area of the beam cross section is denoted by A and ρ is the density of the isotropic material. The equation of motion is

$$EI\frac{\partial^4 v(x,t)}{\partial x^4} + P\frac{\partial^2 v(x,t)}{\partial x^2} + \rho A\frac{\partial^2 v(x,t)}{\partial t^2} = 0 \qquad (2.2.1)$$

First, separation of variables is used to arrive at the spatial equation in the form of an ordinary differential equation. The solution of the spatial equation yields the general form of the eigenfunction, or mode shape. The mode-shape of the first segment of the beam, which is given in Aydin (2008), is

$$X_1(x) = X(0)\bar{S}_1(x) + \phi(0)\bar{S}_2(x) - \frac{M(0)}{K_b}\bar{S}_3(x) - \frac{V(0) + P\phi(0)}{K_b}\bar{S}_4(x) \tag{2.2.2}$$

Here, *X(0), Φ(0), M(0),* and *V(0)* are the displacement, rotation, moment , and shear force at the fixed end of the beam. The multiplication of modulus of elasticity and moment of inertia is described by K_b. Using the notation of Aydin (2008)

$$\lambda^2 = \frac{P}{2K_b} \qquad k^4 = \frac{\bar{m}w^2}{K_b} \qquad K_b = EI \qquad \bar{m} = \rho A \tag{2.2.3}$$

$S_i(x)$ are linearly independent solutions that come from the physical properties of the system as well as the tensile loading. The Function $S_i(x)$ are given as

$$\begin{aligned} S_1(x) &= \sin(k_1 x) \\ S_2(x) &= \cos(k_1 x) \\ S_3(x) &= \sinh(k_2 x) \\ S_4(x) &= \cosh(k_2 x) \end{aligned} \tag{2.2.4}$$

k_1 and k_2 are considered to be

$$\begin{aligned} k_1 &= \lambda\sqrt{1 + \sqrt{1 + (\frac{k}{\lambda})^4}} \\ k_2 &= \lambda\sqrt{-1 + \sqrt{1 + (\frac{k}{\lambda})^4}} \end{aligned} \tag{2.2.5}$$

The force and displacement on both sides of the crack are considered to be equal. The continuity across the crack is enforced by the following conditions.

$$
\begin{aligned}
&X_{i+1}(x_i) = X_i(x_i), \\
&V_{i+1}(x_i) = V_i(x_i) \\
&M_{i+1}(x_i) = M_i(x_i) \\
&X'_{i+1}(x_i) = X'_i(x_i) + C_i X''_i(x_i)
\end{aligned}
\tag{2.2.6}
$$

Where x_i is the position of the crack, and C_i is considered to be the local flexibility, or compliance, introduced by the crack.

Compliance is described by the empirical equation given in Aydin (2008) as

$$C_i = 5.346hf(a_i / h) \tag{2.2.7}$$

This function describes the local rotational stiffness induced by the crack with the crack depth given as a_i, and the height of the beam as h.

The function $f(a_i/h)$ is computed from the strain energy function given in Dimarogonas (1996).

$$
\begin{aligned}
&f(a_i / h) = 1.862(a_i / h)^2 - 3.95(a_i / h)^3 \\
&+16.375(a_i / h)^4 - 37.226(a_i / h)^5 + 76.81(a_i / h)^6 \\
&-126(a_i / h)^7 + 172(a_i / h)^8 - 143.97(a_i / h)^9 + 66.56(a_i / h)^{10}
\end{aligned}
\tag{2.2.8}
$$

The general mode shape of the segment of beam after the first crack is given by Aydin (2008) as

$$X_2(x) = X_1(x) + C_1 X''_1(x_1)\bar{S}_2(x - x_1)H(x - x_1) - \frac{P}{K_b} C_1 X''_1(x_1)\bar{S}_4(x - x_1)H(x - x_1) \tag{2.2.9}$$

Smallest Crack Detectable in a Cantilever Beam

This analysis will attempt to determine the smallest crack that the natural frequency method can determine. The smallest detectable crack is considered to be one that shifts the natural frequency by at least half of a hertz because half of a hertz is usually taken as the measurement sensitivity. The beam that is numerically analyzed is a cantilever beam with boundary conditions as described by

$$\phi(0) = 0$$
$$X(0) = 0$$
$$X''_{n+1}(L) = 0$$
$$K_b X'''_{n+1} + P X'_{n+1}(L) = 0 \tag{2.2.10}$$

Using these conditions the mode shape of the first segment of a cantilever beam can be found to be

$$X_1(x) = -\frac{M(0)}{K_b}\bar{S}_3(x) - \frac{V(0)}{K_b}\bar{S}_4(x) \tag{2.2.11}$$

From the boundary conditions, the equation of motion, and the mode shapes, the conditions

$$-\frac{M(0)}{K_b}\overline{S''_3}(L) - \frac{V(0)}{K_b}\bar{S}''_4(L) + C_1 X''_1(x_1)[\bar{S}''_2(L - x_1) - \frac{P}{K_b}\bar{S}''_4(L - x_1)] = 0 \tag{2.2.12}$$

and

$$-[\overline{S'''_3}(L) + \frac{P}{K_b}\overline{S'_3}(L)]M(0) - [\bar{S}'''_4 + \frac{P}{K_b}\bar{S}'_4(L)]V(0) + c_1 X''_1(x_1)[K_b\{\bar{S}'''_2(L - x_1) -$$
$$\frac{P}{K_b}\bar{S}'''_4(L - x_1)\} + P\{\bar{S}'_2(L - x_1) - \frac{P}{K_b}\bar{S}'_4(L - x_1)\}] = 0 \tag{2.2.13}$$

must be satisfied.

The second derivative of $X_1(x_c)$ is

$$X''_1(x_1) = -\frac{\bar{S}''_3(x)}{K_b}M(0) - \frac{\bar{S}''_4(x)}{K_b}V(0) \tag{2.2.14}$$

Substituting X_1'' into equations (2.2.12) and (2.2.13) and Factoring out $V(0)$ and $\phi(0)$ yields

$$[-\frac{\bar{S}_3''(L)}{K_b}+c_1[\bar{S}_2(L-x_1)-\frac{P}{K_b}\bar{S}_4''(L-x_1)][-\frac{\bar{S}_3''(x_1)}{K_b}]]M(0)+$$
$$[-\frac{\bar{S}_4''(L)}{K_b}+c_1[\bar{S}_2(L-x_1)-\frac{P}{K_b}\bar{S}_4''(L-x_1)][-\frac{\bar{S}_4''(x_1)}{K_b}]]V(0)=0 \tag{2.2.15}$$

And

$$[-\bar{S}_3'''(L)-\frac{P}{K_b}\bar{S}_3'(L)+c_1[K_b\{\bar{S}_2'''(L-x_1)-\frac{P}{K_b}\bar{S}_4'''(L-x_1)\}+$$
$$P\{\bar{S}_2'(L-x_1)-\frac{P}{K_b}\bar{S}_4'(L-x_1)\}][-\frac{S_3''(x_1)}{K_b}]]M(0)+$$

$$[-\bar{S}_4'''(L)-\frac{P}{K_b}\bar{S}_4'(L)+c_1[K_b\{\bar{S}_2'''(L-x_1)-\frac{P}{K_b}\bar{S}_4'''(L-x_1)\}$$
$$+P\{\bar{S}_2'(L-x_1)-\frac{P}{K_b}\bar{S}_4'(L-x_1)\}][-\frac{\bar{S}_4''(x_1)}{K_b}]]V(0)=0 \tag{2.2.16}$$

Equations (2.2.15) and (2.2.16) can then be written in matrix form

$$\begin{bmatrix} [-\frac{\bar{S}_3''(L)}{K_b}+c_1[\bar{S}_2(L-x_1)- \frac{P}{K_b}\bar{S}_4''(L-x_1)][-\frac{\bar{S}_3''(x_1)}{K_b}]], & [-\frac{\bar{S}_4''(L)}{K_b}+c_1[\bar{S}_2(L-x_1)- \frac{P}{K_b}\bar{S}_4''(L-x_1)][-\frac{\bar{S}_4''(x_1)}{K_b}]] \\ [-\bar{S}_3'''(L)-\frac{P}{K_b}\bar{S}_3'(L)+c_1[K_b\{\bar{S}_2'''(L-x_1)-\frac{P}{K_b}\bar{S}_4'''(L-x_1)\}+ P\{\bar{S}_2'(L-x_1)-\frac{P}{K_b}\bar{S}_4'(L-x_1)\}][-\frac{S_3''(x_1)}{K_b}]], & [-\bar{S}_4'''(L)-\frac{P}{K_b}\bar{S}_4'(L)+c_1[K_b\{\bar{S}_2'''(L-x_1)-\frac{P}{K_b}\bar{S}_4'''(L-x_1)\} +P\{\bar{S}_2'(L-x_1)-\frac{P}{K_b}\bar{S}_4'(L-x_1)\}][-\frac{\bar{S}_4''(x_1)}{K_b}]] \end{bmatrix}\begin{bmatrix} M(0) \\ V(0) \end{bmatrix}=0$$

By taking the determinant of this matrix and setting it equal to zero the frequency equation is established. The roots of the characteristic equation are the eigenvalues which are the squares of the natural frequencies.

Analytical Calculations

By using a numerical integration code, (Mathematica), the procedure presented by Aydin (2008) was completed and the first natural frequency was established. The Mathematica code used is given in Appendix A**.** Iteration was performed on the crack length to determine how large of a crack is necessary to induce a 0.5 Hz frequency shift.

The beam to be used in this analysis is made of aluminum and the dimensions are given in figure 2.2.1. This beam is of the same properties and dimensions as the beam in the experimental study contained in this thesis. The modulus of elasticity for aluminum is 71.7 GPa and the mass density is 2700 kg/m^3 (taken from Shigley (2004)).

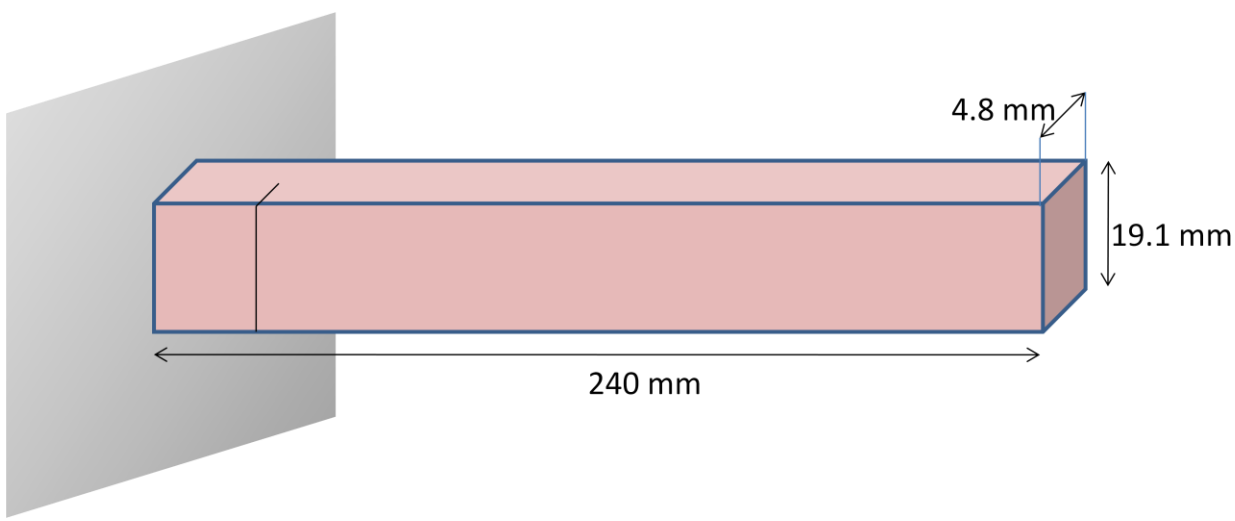

Figure 2.2. 1 Dimensions of experimental beam used in natural frequency analytical study

A graph of how the first natural frequency of the beam changes with crack size is given in Figure 2.2.2. A zoomed in plot shows how the natural frequency changes at the earliest levels of cracking in figure 2.2.3. Detectable damage size is found to be 0.6 mm.

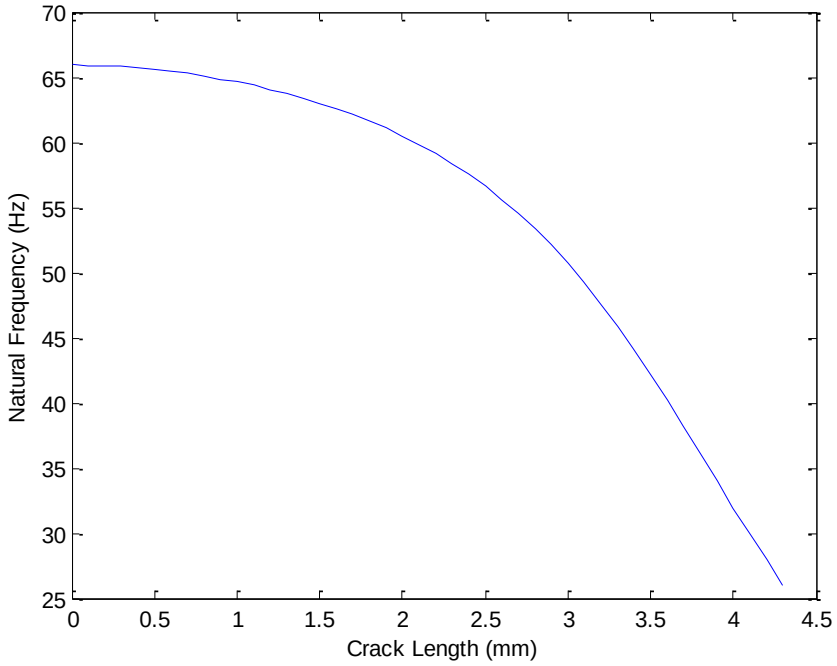

Figure 2.2. 2 Plot of how the first natural frequency shifts with cracking

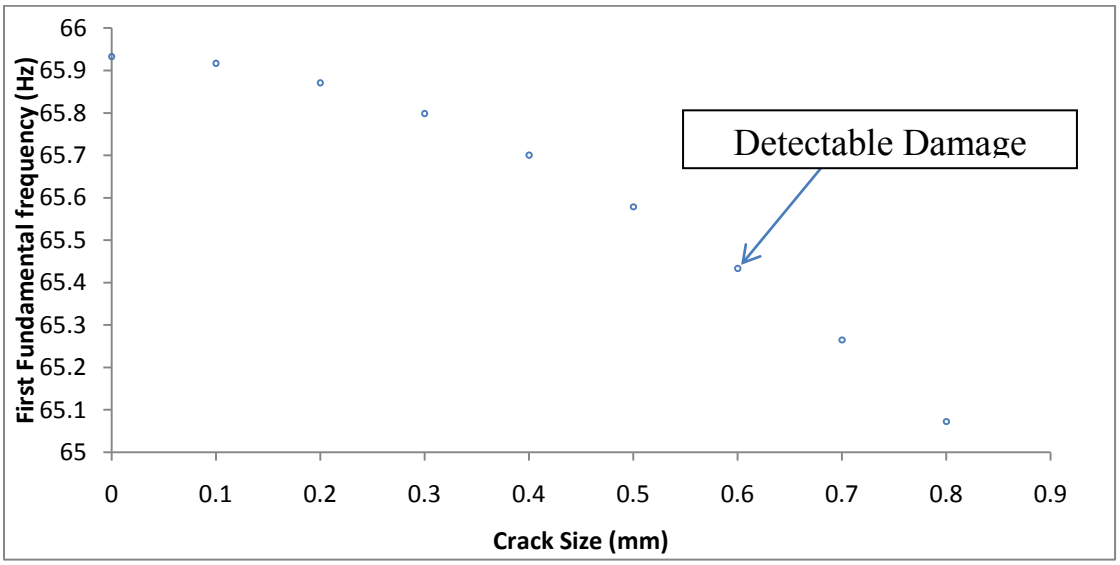

Figure 2.2. 3 Zoomed in plot of first natural frequency showing detectable crack

Through this analysis it was found that the crack must be approximately 12.5% of the thickness in order to induce a frequency shift of 0.5 hertz (π rad/sec) in the first natural frequency. This is a crack of 0.6 mm for this beam. This model will be experimentally investigated in Chapter 3 to verify the detectable crack size. Cracks may be detected earlier or later with other geometries and boundary conditions.

2.3 Temperature Dependent Natural Frequency Model

It is well known that the temperature effects on natural frequency are likely to cause false alarm damage signals in a frequency based SHM system. The modulus of elasticity of a metal is directly affected by temperature. The material becomes stiffer as the temperature decreases and softer as the temperature increases. This will in turn mean that the natural frequency will increase with decreasing temperature and conversely it will decrease with increasing temperature. To be confident that the measurements made in our laboratory setting have not been confounded by small changes in ambient temperature, an analysis on the effect of temperature on our experimental beam is required. The effect of temperature on Young's Modulus of aluminum is given at http://www.engineeringtoolbox.com/young-modulus-d_773.html.

Using this information and the equation for natural frequencies of cantilever beams, the natural frequency can be calculated over a range of temperature. The natural frequencies are calculated from basic equations (See Inman (2001)). The procedure for calculating natural frequency of a beam will now be outlined.

The first natural frequency of a cantilever beam is

$$\omega = \beta^2 \sqrt{\frac{EI}{\rho A}} \ . \tag{2.3.1}$$

In this equation β is a constant, determined by the boundary conditions, and given in Table 6.4 of Inman (2001). In this equation E is the modulus of elasticity, A is the cross sectional area, I is the area moment of inertia, and ρ is the mass density of the material (2700 kg/m^3). For the first natural frequency β is given as

$$\frac{1.87510407}{l}. \tag{2.3.2}$$

where l is the length of the beam. The dimensions of the cantilever beam are found in figure 2.2.1. Using these properties, and the temperature dependent modulus of elasticity, the natural frequencies are computed at a variety of temperatures. The results are presented in figure 2.3.1.

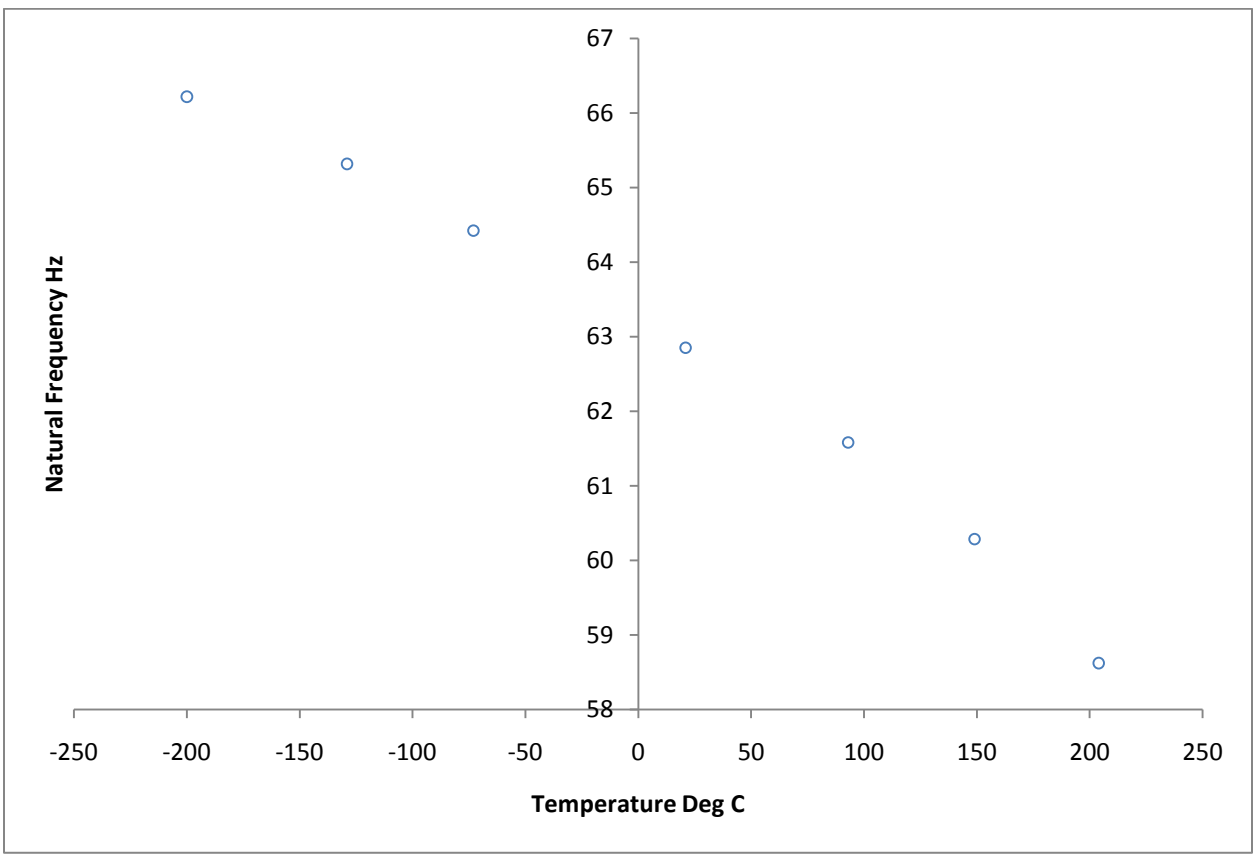

Figure 2.3. 1 Theoretical effect of temperature on the natural frequency of experimental cantilever beam

From the plot it can be determined from the calculated natural frequency values that the theoretical change in first natural frequency per change in degree Celcius is -0.018797. This means that about 27 degree Celsius change in temperature is required for a change in frequency of 0.5 Hertz. This is a change in frequency of about 1.88 hertz over a 100 C change in temperature. From this it can be concluded that it is unlikely that the change in temperature in a lab environment will significantly effect the natural frequencies for a cantilever beam. However, in an outdoor environment this effect will need to be accounted for. It should be noted that beams with different boundary conditions will be effected differently. Beams with fixed-fixed boundary conditions and pinned-pinned boundary conditions will be effected in a much greater way than the cantilever beam used in this study due to the clamping effect of the boundary conditions. An experiment has been designed to validate the theory and will be presented in chapter 3.

2.4 Beat Phenomena

The beat method is considered because it is known to magnify small difference in frequencies of signals in the time domain and may be more sensitive than frequency domain measurements of frequency shifts. The beat method does not require any analytical model, however we can analytically determine how much the natural frequency must shift in order to cause beating. This will be done by simulating two free decay signals in Matlab with the frequencies expected for our experimental beam. By iterating the difference in frequency between the signals we can determine the smallest shift which will cause beating to occur. It has been presented in Cattarius (2000) that a shift of at least 0.4% in frequency will cause beating to occur. Since our beam is predicted to have a first natural frequency of 65.78 Hz, a shift of 0.26 Hz should cause beating. Beating should occur at a frequency of 65.52 Hz.

The dimensions of the aluminum beam used in this analytic study are found in Figure 2.2.1**.** The modulus of elasticity for aluminum is 71.7 GPa and the mass density is 2700 kg/m^3 (per Shigley (2004). The boundary conditions are cantilever in order to compare with the previous results. A free decay signal will be simulated in Matlab at 65.78 Hz as well as other lower frequencies. By doing a subtraction technique we can determine the smallest shift in frequency that will cause beating. The code used to perform this analysis is given in Appendix A**.** The plots of the subtraction of a signal from the baseline are given in figures 2.4.1 through 2.4.6. These plots show beating occuring at a frequency shift of 0.2 Hz. This is a 0.3 percent change in natural frequency and shows a significant improvement over the 0.5 Hz detectable shift in frequency using frequency domains. It can be concluded that the method of using time series data and the beat phenomenon has potential to detect smaller damage than the frequency domain method. This method will be verified and compared with the natural frequency domain method experimentally in Chapter 3.

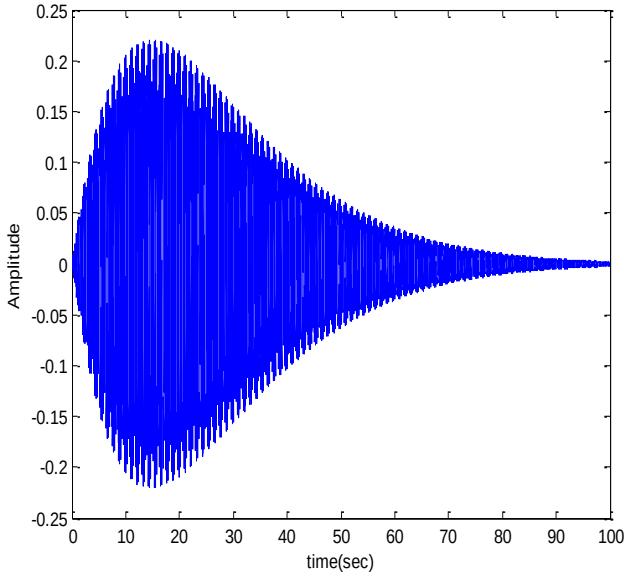

Figure 2.4. 1 Analytical Beat Frequency (Baseline signal – 65.74 Hz Signal)

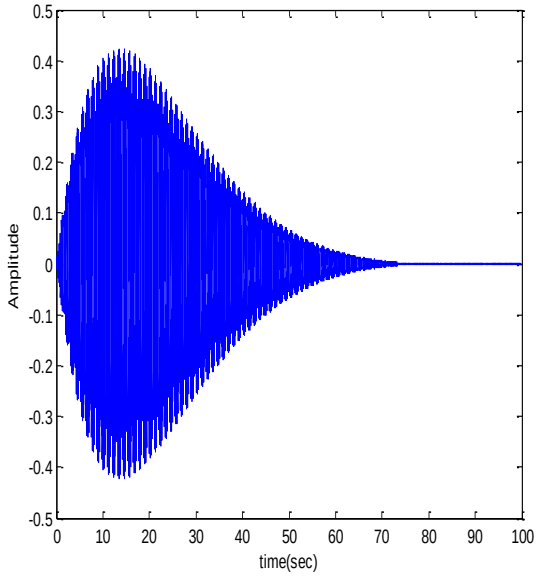

Figure 2.4. 2 Analytical Beat Frequency (Baseline signal – 65.70 Hz Signal)

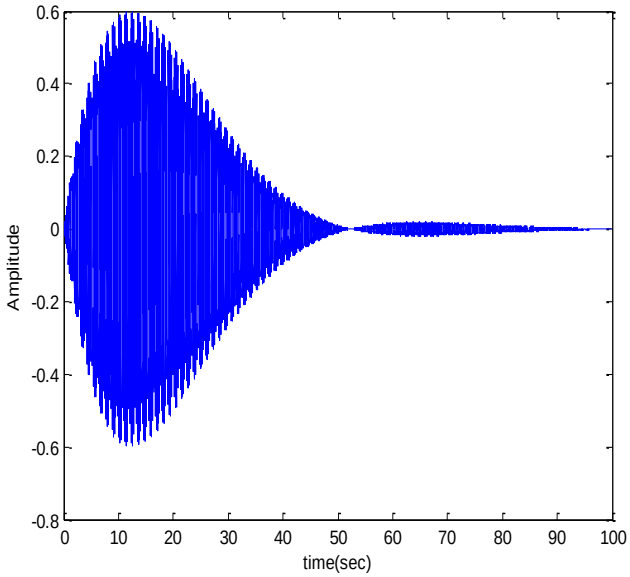

Figure 2.4. 3 Analytical Beat Frequency (Baseline signal – 65.66 Hz Signal)

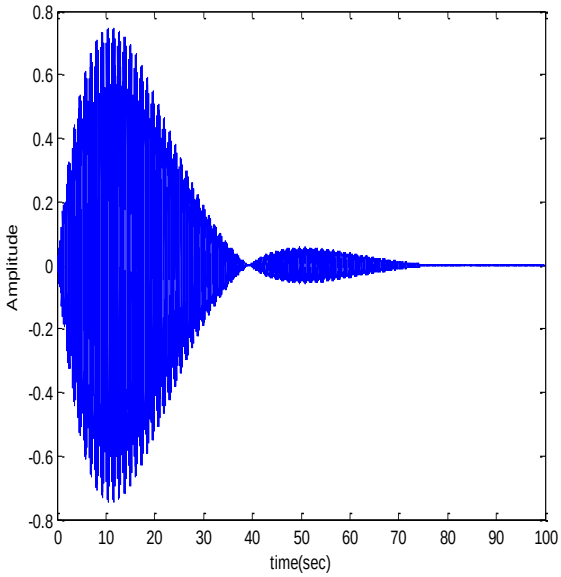

Figure 2.4. 4 Analytical Beat Frequency (Baseline signal – 65.62 Hz Signal)

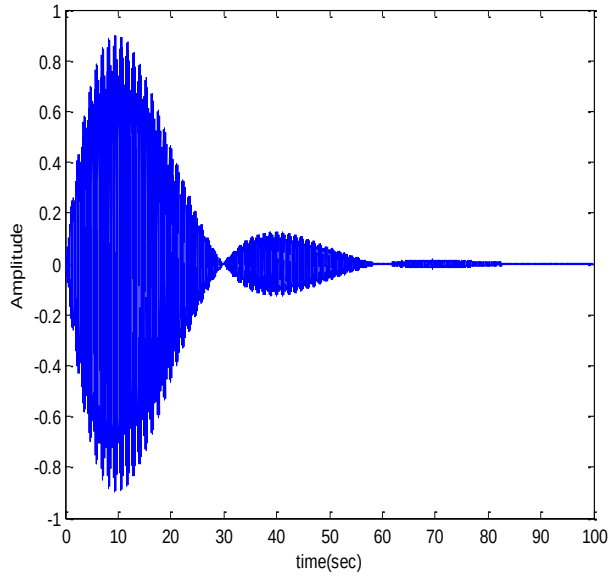

Figure 2.4. 5 Analytical Beat Frequency (Baseline signal – 65.58 Hz Signal)

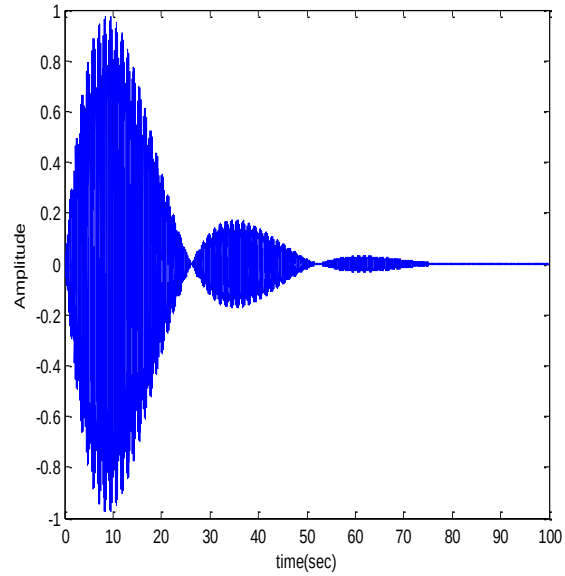

Figure 2.4. 6 Analytical Beat Frequency (Baseline signal – 65.54 Hz Signal)

2.5 Analytical Model for calculation of SIF

Stress intensity factors are important parameters in fracture mechanics that are used to estimate incipient fracture as well as the remaining service life of structures. Although the analytical solution of SIF for simple structures is readily available, the calculation of stress intensity factors for complex structures is expensive. A method of measuring SIF would be beneficial as the measurements could be used instead of using the complicated and expensive models to predict failure. An analytical model for calculation of stress intensity factors for a beam specimen that will be experimentally verified later in the thesis is presented here. The model is necessary to ensure that the stress intensity factors calculated from the experimental data are accurate. Once

the algorithm for calculating stress intensity factors from measured voltages is verified, the method can be applied to more complex structures.

One analytical model for calculating the mode-I stress intensity factor, denoted as *Ki*, due to a sharp crack is given in Ashby (1999) as:

$$Ki = C\sigma\sqrt{\pi a} \qquad 2.5.1$$

~~Where~~ In this equation, σ is the nominal stress in the beam. The factor C is a function of the beam width, w, and the crack length, a, and is given by:

$$C = \frac{1.1(1-0.2\left(\frac{a}{w}\right))}{(1-\frac{a}{w})^{3/2}} \qquad 2.5.2$$

for the for the simple beam shown in figure 3.5.3**.**

Performing this analysis on our experimental beam we can track how the mode ~~one~~ 1 SIF, which is typically called the tearing mode, will change with a growing crack. The aluminum beam used in our experiment is 226 mm in length, 25.4 mm in width and 3.175 mm in thickness. A graph of how the theoretical ~~*K1*~~ *Ki* stress intensity factor is expected to grow with crack length is given ~~below~~ in Figure 2.5.1. ~~*K2*~~ *Kii* is the mode 2 SIF, which is typically called the sliding mode, and is predicted to be ~~0~~ zero for the case of axial loading.

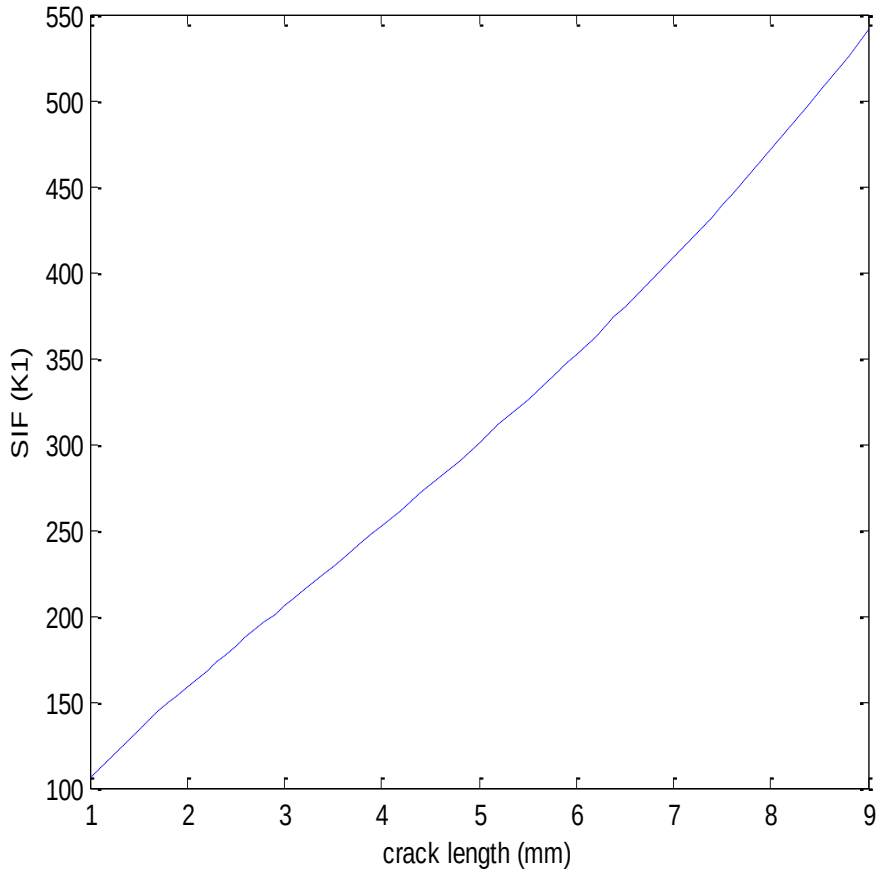

Figure 2.5. 1 Theoretical SIF vs. Crack Length for Experimental Geometry

~~plane stress.~~Chapter 3: Experimental Verification

3.1 Experimental Verification of Crack model

3.1.1 Saw Cut Damage

Motivation: Previously in this manuscript an Euler-Bernoulli beam model which takes into account cracks was evaluated analytically. From this model it was determined how large of a crack is necessary to induce a frequency shift of 0.5 Hz for beams of different dimensions. The beam of most interest is of the dimensions of the cantilever beam in the experimental study. For this beam a crack of 0.6 mm was analytically determined to induce the necessary frequency shift. The dimensions of the beam are given in the experimental set up section. The experiment is designed to test for correlation of the physical system to the analytical model. This reinforces and validates our claim of a necessary size of the damage for significant frequency shift. The beam is actuated by a piezoceramic and the resulting mechanical vibrations are analyzed by a laser vibrometer. This is done using frequency analysis. The mode of damage is a saw cut.

Set up: In this experiment the change of natural frequency due to a saw cut is monitored. The cantilever beam is mounted in a test mount as shown in figure 3.1.1. The beam is 24 cm long with height of 19.1 mm and a base of 4.8 mm. A PSI-5A4E piezoceramic patch is mounted to the cantilever near the base. The ceramic is first cut to the appropriate size and then bonded to the aluminum using super glue. In this experiment the beam is cut with a coping saw, at the location 1.5 cm from the base, to induce damage. The changes in natural frequency are monitored to detect damage. The crack size is measured using a laser proximity probe.

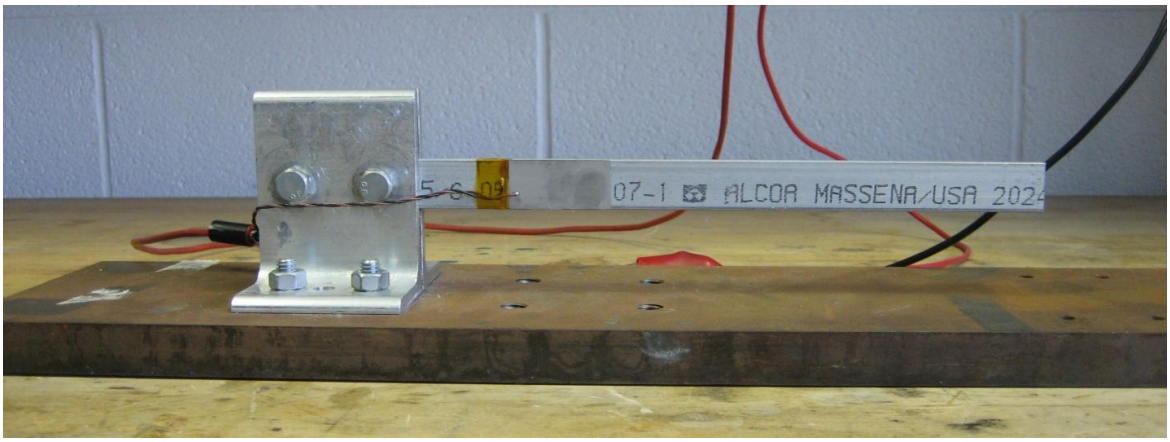

Figure 3.1. 1 Experimental set up showing cantilever beam with piezoceramic wafer

Procedure: The frequency response function (FRF) is used to determine shifts in the first two fundamental frequencies of the beam. The FRF is found by actuating the piezoceramic using a burst chirp signal from 1-500 Hz. The amplitude of the signal generated by the SigLab is 0.5 volts peak to peak. It is then run through a Trek HV power supply, model 50/750, with a gain of 19.7. This gives about 10 volts peak to peak actuation of the piezoceramic. The response is measured using a laser vibrometer. The bandwidth of the measurement is 500Hz. The record length is 8192. Five response functions are averaged to compute the FRF. The goal is to determine how big of a crack is necessary to induce a frequency shift of 0.5 Hz. Using a laser vibrometer yields measurements which have a greater resolution than half of a hertz, however, SHM methods of measurements such as a piezoelectric sensor will only be able to detect shifts of at least half of a hertz. This is a rule of thumb used by experimentalists that takes into account uncertainty in measurements as well as signal processing.

The experiment is conducted twice using two different directions of saw cut. One mode of cracking is in the same plane as the PZT and the other is perpendicular. It should be noted that

the model used for the transverse vibration of the beam is for the in plane crack and will not accurately predict the natural frequency shifts due to an out of plane crack.

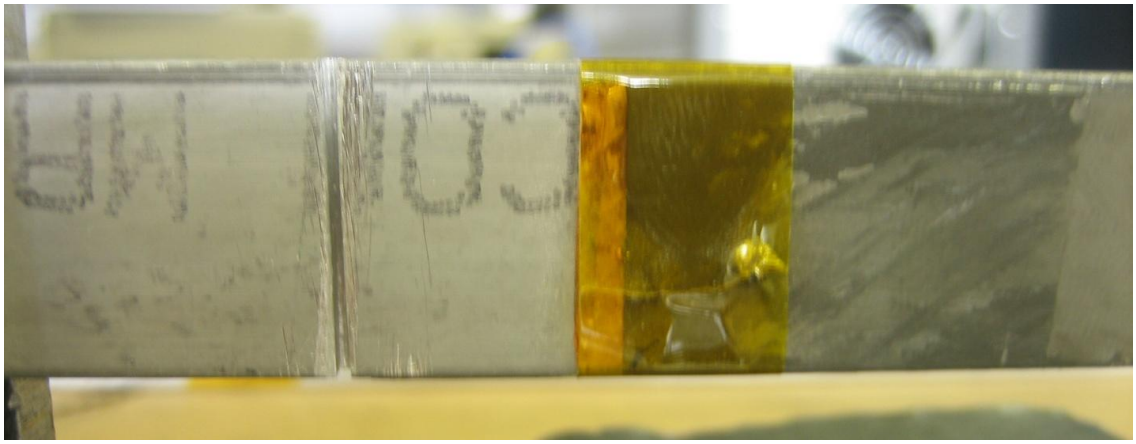

Figure 3.1. 2 Picture of saw cut in plane with the attachment of PZT

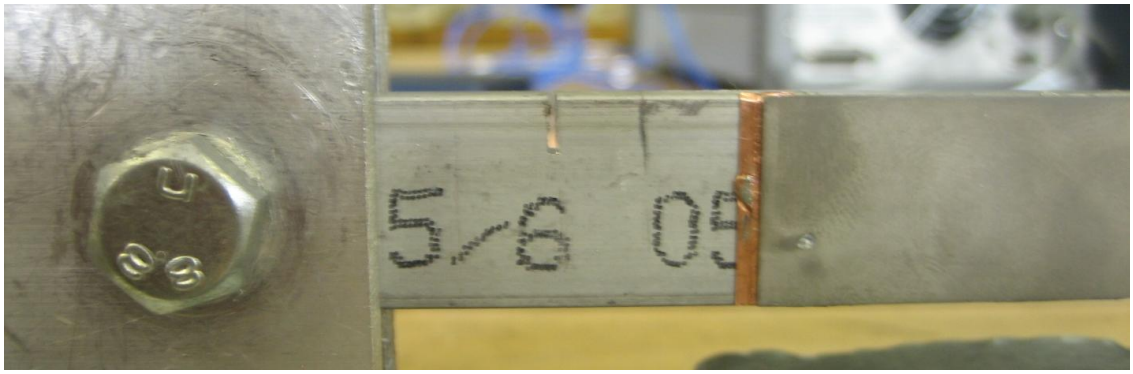

Figure 3.1. 3 Picture of saw cut out of plane with the attachment of PZT

The levels of cracking used in each experiment are given in Tables 3.3.1 and 3.3.2.

Results for in-plane test: For the in-plane test it was found that the shift in the first natural frequency was predicted quite well by the analytical model. The frequency spectrums measured are presented in Appendix B. An overlaid plot of how the first two natural frequencies shift due

to cracking is given in Figure 3.1.4. A plot of how the first natural frequency changes with cracking is presented in Figure 3.1.5. From this figure we can see that the experimental data matches the analytical data quite well. A saw cut with a depth between 0.7mm and 1 mm is necessary to induce a frequency shift of 0.5 Hz in the first frequency. It was also found that a saw cut of between 0.3 mm and 0.7 mm is necessary to shift the second frequency by the same 0.5 Hz. Therefore the detectable damage, at this location, for the in-plane case, is a saw cut of between 0.3m and 0.7 mm, or between 6.2 and 14.5% of the thickness of the beam. Although this does not seem like a very large cut, saw cut damage is a relatively severe type of damage compared with the more common damage of fatigue.

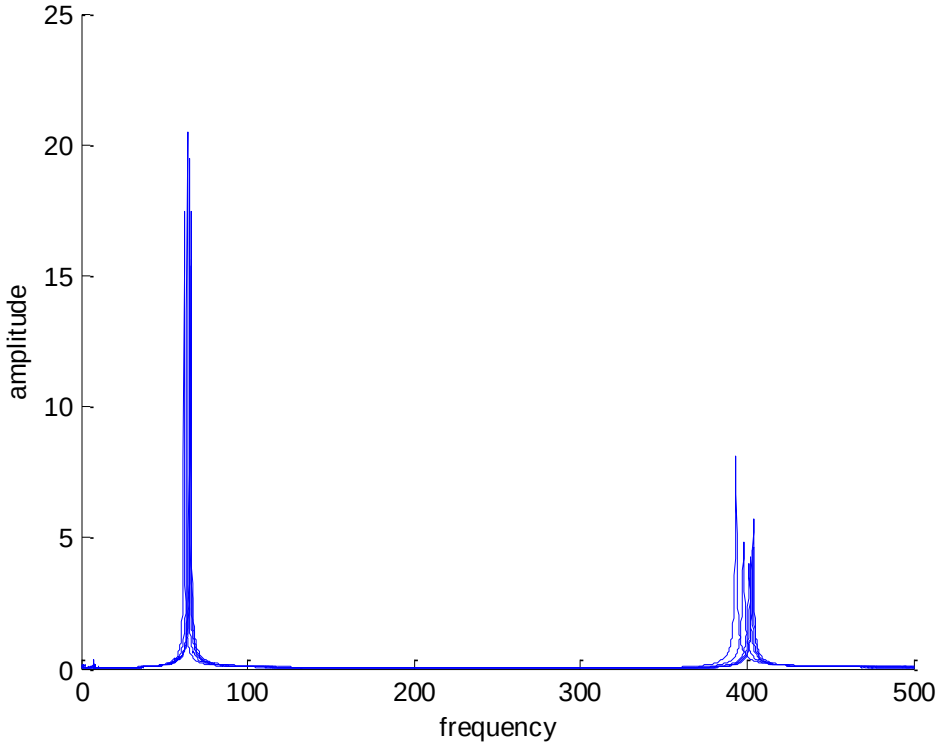

Figure 3.1. 4 Overlaid Plot of Frequency response functions for all cases of in plane damage

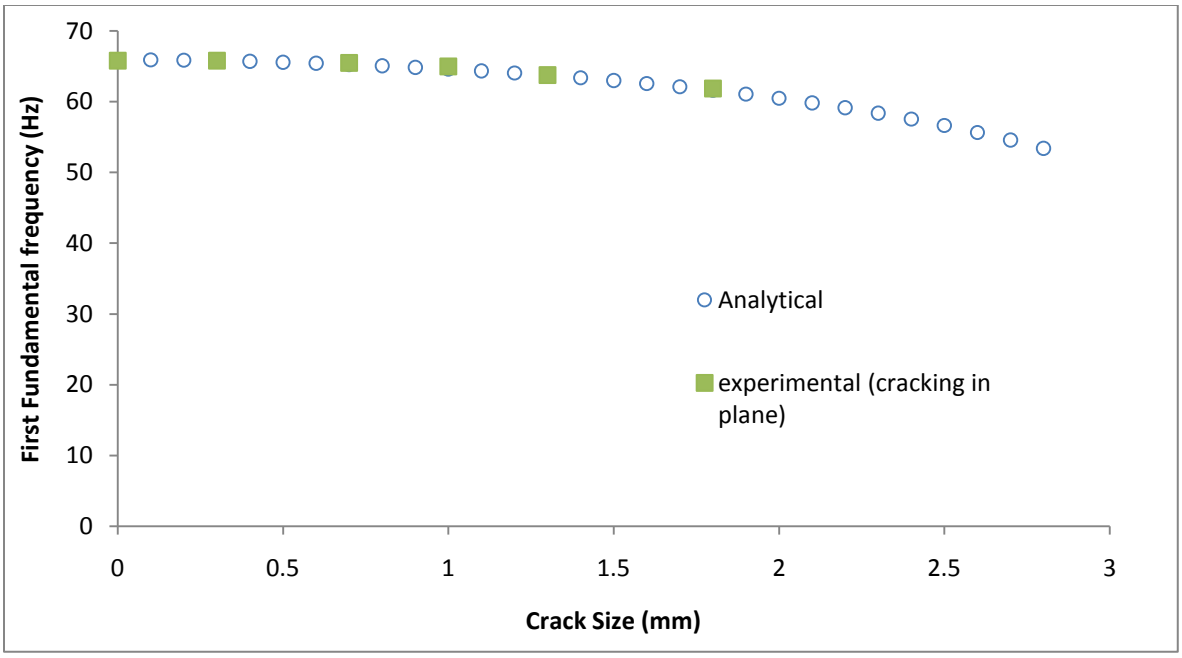

Figure 3.1. 5 Plot of how first natural frequency changes with in plane damage

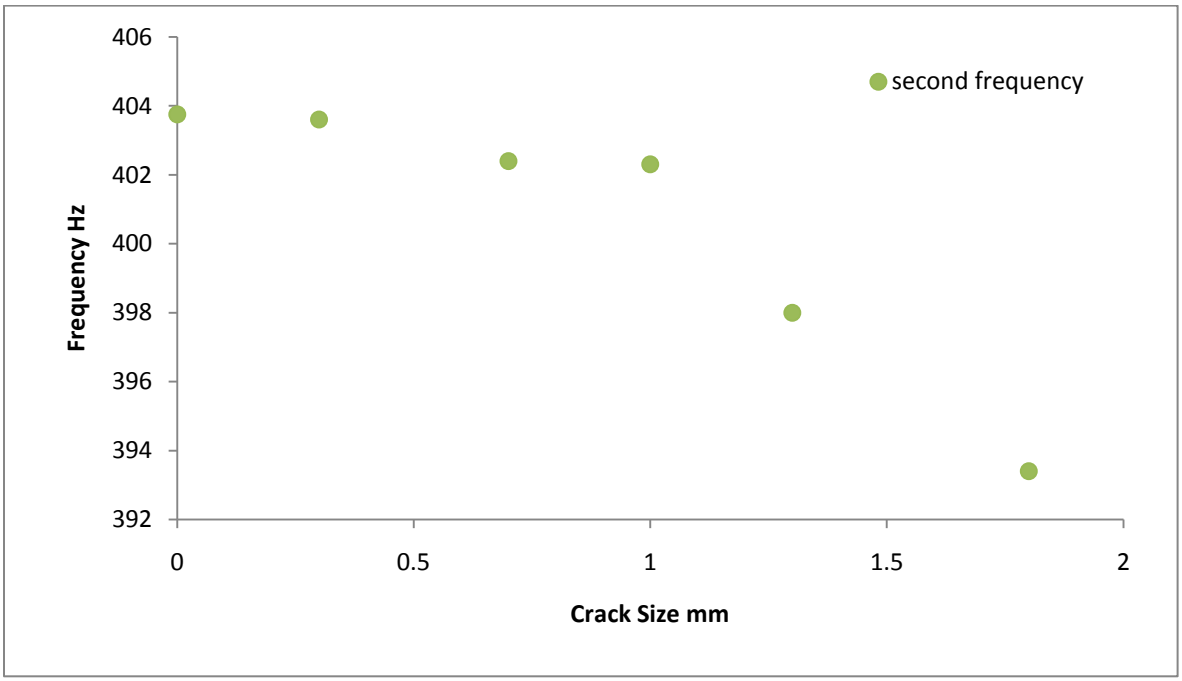

Figure 3.1. 6 Plot of how second frequency changes with in-plane damage

Results for out of plane test: The analytical model does not accurately predict the shifts in frequencies due to cracking. This is due to the direction of actuation and measurement. The beam has different stiffness, and therefore resonant frequencies, due to different directions of actuation. If the cut is in the same plane as the actuation, the model will be able to predict the frequency shifts. If the beam is actuated in a different plane than the damage, the model does not accurately predict the frequencies.

A plot of how the first natural frequency will shift experimentally with an out of plane saw cut is given in figure 3.1.7. A plot of how the second frequency shifts with cracking is given in figure 3.1.8. A saw cut of 2.5 mm is necessary to shift the first natural frequency by half of a Hz in the out of plane case which is approximately 13% of the height. A saw cut of 2 mm or approximately 10% of the height is necessary to shift the second frequency by the same 0.5 Hz. This leads us to conclude that a saw cut of 10 % of the height is necessary to be detected when the damage is in the plane perpendicular to the mode of actuation of the PZT wafer.

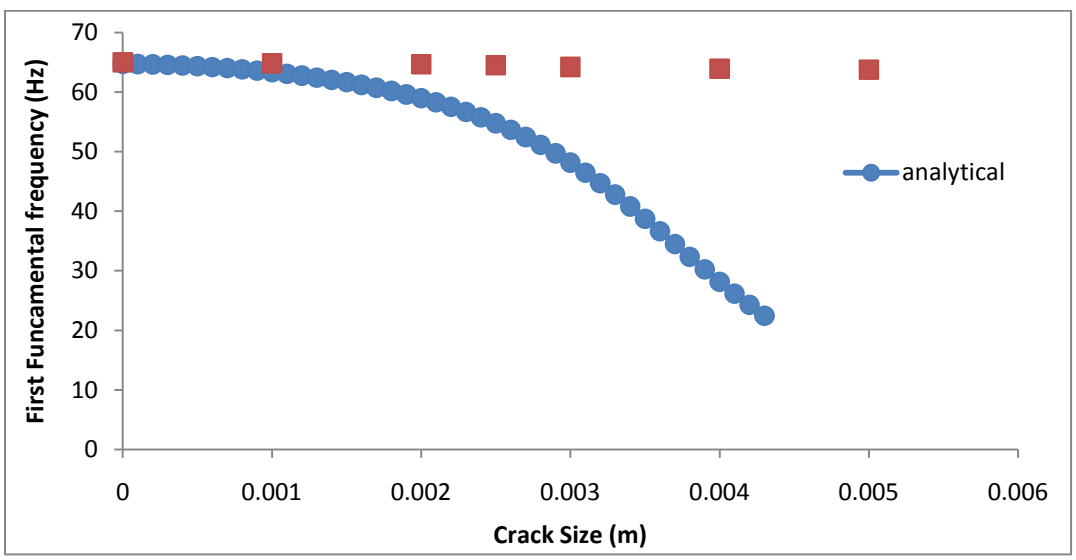

Figure 3.1. 7 Plot of how first natural frequency changes with out of plane cracking

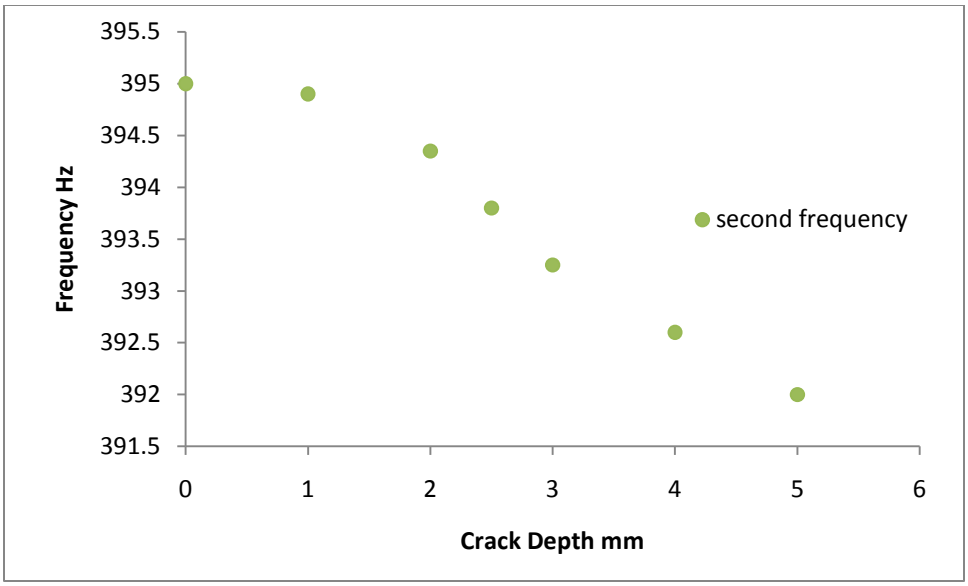

Figure 3.1. 8 Plot of how second natural frequency changes with out of plane cracking

Conclusions

Although the model is not able to predict the shift in frequency due to cracking out of plane, it accurately predicts the in plane crack. From this study it was found that different size cracks are detectable in different planes relative to the plane of actuation. A much smaller crack is detected when the actuation is in the same plane as the crack, however, when the percentage of the beam that the crack has damaged is compared; similar sized damage is detectable in both cases. A crack of about 10% of the thickness or height of the beam is necessary to be detected using natural frequency shifts as damage indicators. Although it was believed that the first frequency of a cantilever beam would be the most affected frequency when the crack was near the fixed end of the beam, this was not found to be the case. The second frequency was affected with a greater magnitude in both cases of damage. A 0.5 Hz shift in the first natural frequency of 65.7 Hz is a change of 0.76%. A 0.5 Hz shift in the second frequency of 395 Hz is a change of

0.127%. Therefore a larger percent shift in frequency is necessary to be detectable in the first mode than the second mode.

3.2 Temperature dependent natural frequency study

Motivation: An experiment was designed to determine the effect of temperature on the natural frequency of the cantilever beam used in the saw cut experiment. The objective is to determine the temperature shift that causes a 0.5 hertz shift in natural frequency. This is done in order to determine whether changes in ambient temperature could be confounding the natural frequency shifts measured during the saw cut experiment. We know that temperature is a significant factor in natural frequencies of metal structures. In depth analysis into the effect of temperatures on the physical properties of metals is necessary to avoid false alarms during in situ applications of vibration based SHM and NDE methods. Although it has been suggested that comparing measurements at the same time of year is another way to avoid environmental factors, SHM systems would most likely require weather sensing and compensation techniques.

Set up: The cantilever beam is prepared the same way as in the saw cut experiment. The dimensions of the beam are the same as in the previous experiment to ensure continuity: 226 mm in length, 25.4 mm in width and 3.175 mm in thickness. As before a PZT ceramic patch is attached near the base of the beam for actuation. Although in an SHM system another PZT would be useful for sensing, a laser Vibrometer is used to measure the vibration signatures. The beam is placed in a Tenney Versa Tenn III environmental chamber (model 36-ST) which is able to vary temperature as well as pressure. The laser measurements are taken through a window in the chamber door.

Procedure: The frequency response function (FRF) is used to determine shifts in the first fundamental frequency of the beam. The FRF is found by actuating the piezoceramic wafer

using a burst chirp signal from 1-500 Hz. The amplitude of the signal is 0.5 volts, peak to peak, in the Siglab. It is then run through a Trek HV power supply (model 50/750) with a gain of 19.7. The model number is 50/750. This gives about 10 volts peak to peak actuation of the piezoceramic. The response is measured using a laser vibrometer. The bandwidth of the measurement is 500Hz. The record length is 8192. The FRF is computed using an average of five measured responses.

Results and conclusions: Figure 3.2.1 shows how the first natural frequency changes with temperature.

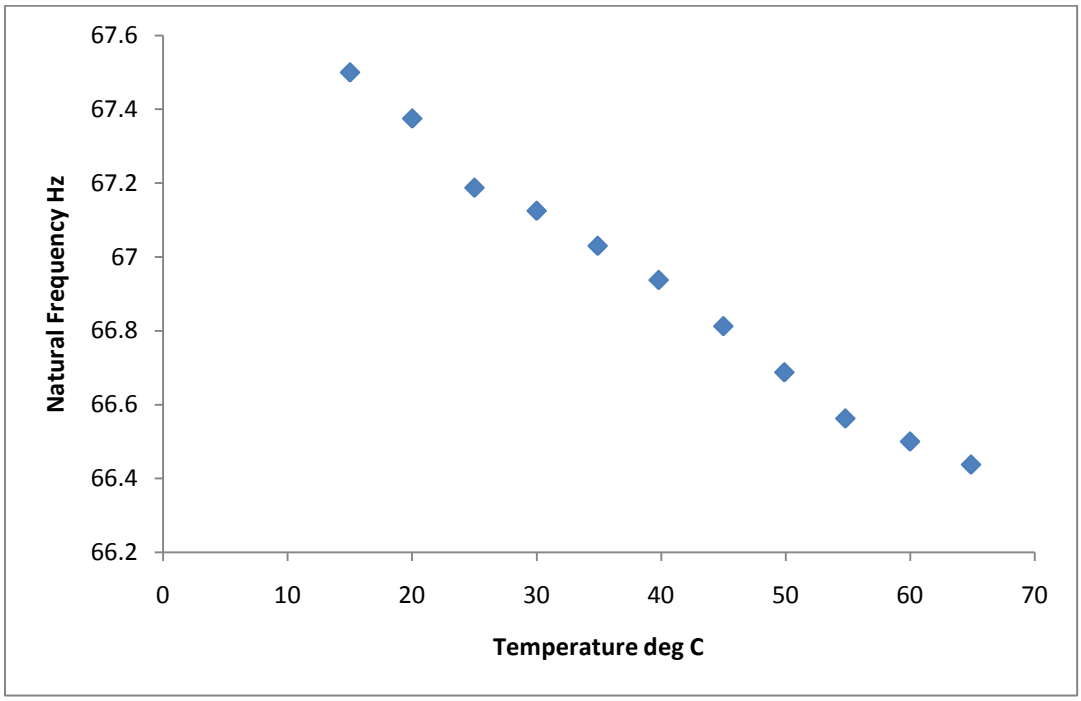

Figure 3.2. 1 Change in first natural frequency due to experimental temperature change

The experimental change in frequency per change in degree C is -0.02129. This means that about 24 C change in temperature is required for a change in frequency of 0.5 Hertz. This is a change in frequency of 2.129 hertz over a 100 C change in temperature. It is not likely that

temperatures in the lab environment will greatly affect our measurements, however in other environments this effect could confound the SHM technique. This is a similar result as was found in the analytical study. Although for cantilever beams the effect of the change in modulus of elasticity does not change the natural frequency greatly, for beams of other boundary conditions this effect will be much greater. We can expect that the effect on a fixed-fixed beam would be the greatest. This can be illustrated by the equations for effective stiffness of beams. The effective stiffness of a cantilever beam from Inman (2001) is

$$K = \frac{3EI}{L^3} \tag{3.2.1}$$

The effective stiffness of a fixed-fixed beam is

$$K = \frac{192EI}{L^3} \tag{3.2.2}$$

If we consider the change in modulus of elasticity to be ΔE, and substitute it into the equations for effective stiffness we get the equations

$$K = \frac{3(E+\Delta E)I}{L^3} \tag{3.2.3}$$

and

$$K = \frac{192(E+\Delta E)I}{L^3} \tag{3.2.4}$$

Which can be expressed as

$$K = \frac{3EI}{L^3} + \frac{3\Delta EI}{L^3} \tag{3.2.5}$$

and

$$K = \frac{192EI}{L^3} + \frac{192\Delta EI}{L^3} \tag{3.2.6}$$

The change in effective stiffness, due to change in elastic modulus, for a cantilever beam is

$$\Delta K = \frac{3I}{L^3} * \Delta E \tag{3.2.7}$$

And for a fully constrained beam the change of stiffness is

$$\Delta K = \frac{192I}{L^3} * \Delta E \tag{3.2.8}$$

This shows that the for a beam of the same dimensions, the change in modulus of elasticity has 64 times more of an effect on the stiffness of the beam when the boundary conditions are fixed-fixed. Therefore, temperature will play a much greater role in the natural frequency of fully constrained beams. It should be noted that the natural frequency of a fixed-fixed beam will be much higher than a similarly sized cantilever beam. When percent change in frequency is taken into account the beams will be effected equally. Percent change of stiffness is given by the formula

$$\%\, change = \frac{\Delta K}{K} * 100 \tag{3.2.9}$$

For a cantilever beam the percent change in stiffness due to a change in modulus of elasticity is

$$\frac{\frac{3I}{L^3} * \Delta E}{\frac{3EI}{L^3}} * 100 = \frac{\Delta E}{E} * 100 \tag{3.2.10}$$

For a fixed-fixed beam the percent change of stiffness will be

$$\frac{\frac{198I}{L^3} * \Delta E}{\frac{198EI}{L^3}} * 100 = \frac{\Delta E}{E} * 100 \tag{3.2.11}$$

In conclusion, the stiffness of a fixed-fixed beam will shift with a greater value than the cantilever beam, however, the percent change of stiffness for both beams will be identical.

3.3 Impedance Experiments

Motivation: The impedance method is an attractive SHM method due to its versatility and applicability to real world structures. It is also sensitive to many types of damage and is capable of detecting small scale damage. Determining how small of a crack can be detected using impedance, relative to the vibration methods is another focus of this analysis. Impedance can also be used to provide a first alarm for the application of the SIF method. After the impedance method detects damage, the SIF method will be used to quantify the severity of the damage.

Calculation of Damage Index for Impedance Method

The impedance method is not model based and therefore requires baseline measurements for calculation of a damage index. Damage indices for the impedance method compare two impedance signatures and output a value which signifies the relative difference in signals. The damage index used in this report is root mean square deviation (RMSD). The formula for RMSD is

$$RMSD\% = \sqrt{\sum_{i=1}^{n} \frac{[\mathrm{Re}(Z_{i,1}) - \mathrm{Re}(Z_{i,2})]^2}{[\mathrm{Re}(Z_{i,1})]^2}} \times 100 \tag{13}$$

RMSD is calculated at each case of damage and is the comparison between each damaged case and the baseline case. $\mathrm{Re}(Z_{i,j})$ is the real part of the ith measured value of the jth impedance signature.

3.3.1 Impedance for Saw Cut on Cantilever Beam

Set up: The experimental set up for the measurement of impedance of a cantilever beam is similar to the set up for the natural frequency study as this experiment was run in parallel. One of the main assertions of this analysis is that many detection algorithms can be used with piezoelectric sensors in order to provide a more robust SHM system. The beam analyzed in this section is of the same dimensions as the other cantilever beam experiments. The dimensions are 226 mm in length, 25.4 mm in width and 3.175 mm in thickness. By using the same size beam we can compare detectable crack sizes. The beam is contained in the test apparatus in the cantilever configuration. A piezoceramic patch is attached near the base of the beam as shown in Figure 3.1.1**.** An HP 4194A impedance analyzer will be used to measure the impedance spectrum of the PZT attached to the host structure.

Procedure: Impedance spectrums are measured at an undamaged state as well as at all damaged states. The frequency range is consistent between measurements and is from 0 Hz to 200K Hz. The resolution is 20Hz. Damage is induced 1.5 cm from the base using a coping saw. As in the natural frequency experimental study, this experiment is carried out for two types of damage. The first type of damage is a cut in the same plane as the piezoelectric. The second type of damage is in a plane perpendicular to the adhesion of the piezoelectric. Pictures of the two types of damage can be seen in Figures 3.1.2 and 3.1.3 respectively.

For the in-plane experiment, damage is induced at levels given in Table 3.3.1. For the out of plane experiment damage levels are given in Table 3.3.2**.** For each case of damage the root mean square deviation damage index is calculated. Impedance measurements are complex meaning they contain both real and imaginary components. The real impedance is used in calculation of the damage index due to its lower sensitivity to environmental factors (see Koo (2007))

Table 3.3. 1: Depth of saw cut for different measurements for in plane damage

Damage Case	Crack depth
1	0.3 mm
2	0.7 mm
3	1 mm
4	1.3 mm
5	1.8 mm

Table 3.3. 2: Depth of saw cut for different measurements for out of plane saw cut damage

Damage Case	Crack Depth
1	1 mm
2	2mm
3	2.5 mm
4	3 mm
5	4mm
6	5 mm

In Plane Results: A typical overlaid plot of impedance signatures as damage increases is given in Figure 3.3.1. The values for the calculation of RMSD damage index are given in Figure 3.3.2.

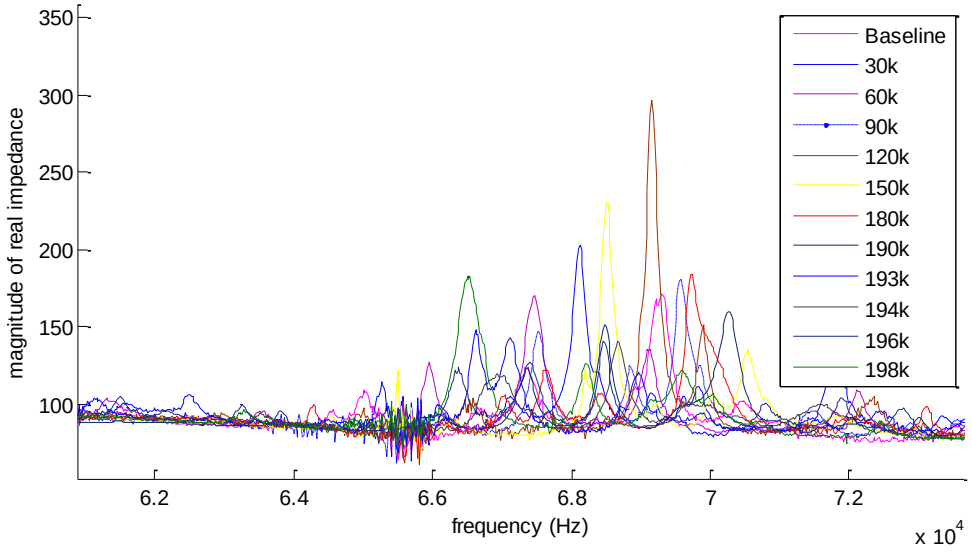

Figure 3.3. 1 Zoomed in Overlaid plot of Impedance signatures at different levels of damage.

.

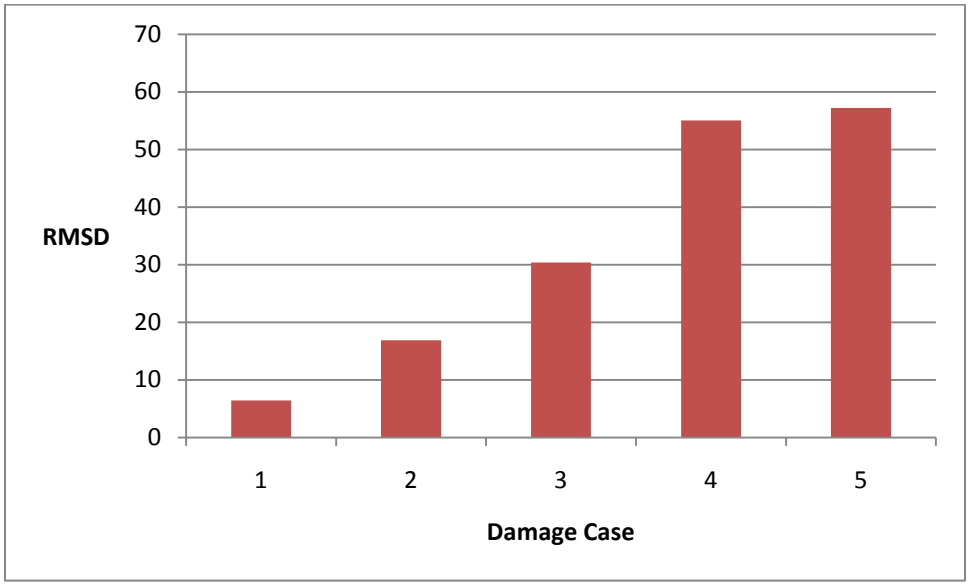

Figure 3.3. 2 RMSD damage index for in plane damage

Out of Plane Results: When the damage is in the plane perpendicular to the plane of actuation of the PZT a slightly different result is obtained. The plot of damage index vs. damage is given in figure 3.3.3. The damage index is affected by the cut; however, the increase in damage index is not monotonically increasing. Since damage case 2 has a higher damage index than later damage cases, it may be difficult to determine whether damage has increased in severity if the crack is out of plane.

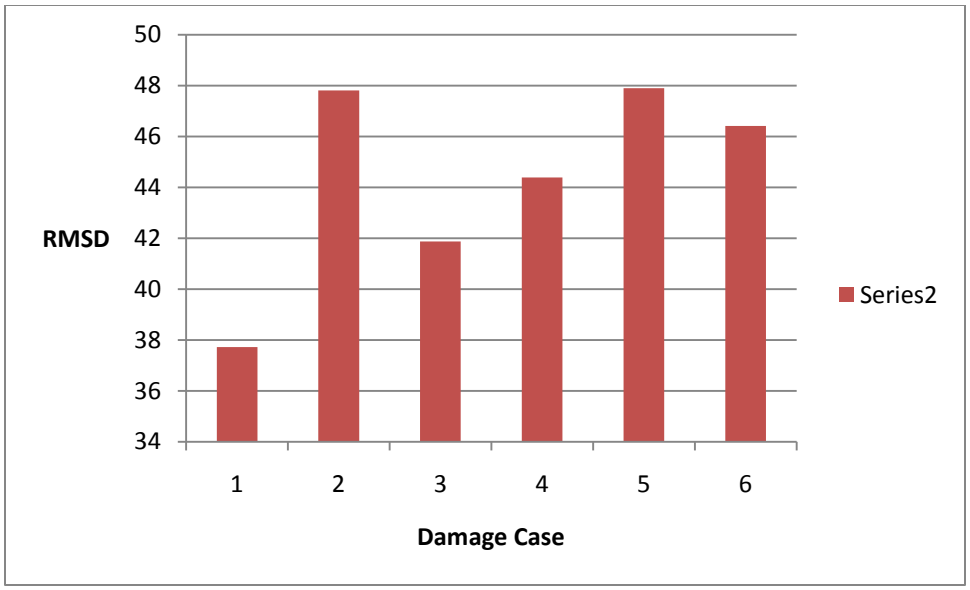

Figure 3.3. 3 RMSD calculations for each case of out of plane damage

Conclusions and Recommendations: From these results it is possible to conclude that a damage of smaller than 0.3 mm in plane saw cut is detectable using the impedance method. We can also detect the first level of out of plane damage. It should be noted that the monotonically increasing damage index found in the in plane experiment is advantageous to the detection algorithm. From this we can see that as the damage increases, so does the damage index. Although there is noted peak attenuation and shifting for the out of plane damage, it does not increase monotonically with damage. This leads us to believe that sensor placement can be important for the impedance method. The placement of the PZT relative to the crack will affect the reliability of the detection algorithm. Although sensor placement is important, the relatively severe damage of saw cut is easily detectable using the impedance method. The impedance method is capable of detecting much smaller damage than the natural frequency method.

3.3.2 Impedance for fatigue of simple Beam

Motivation: Since the impedance method is capable of detecting small size saw cut damage we will now extend this method to the more common damage case of fatigue cracking. Fatigue cracking is a common damage mode in real structures and it would be very advantageous to have a detection algorithm that would be capable of detecting this mode of damage. An experiment has been designed to determine the obstacles involved with detecting fatigue damage in an aluminum beam.

Set up: A beam is fitted with a macro fiber composite (MFC), using a vacuum packing technique with epoxy, for impedance measurement. The active area of the MFC is located 3 mm away from the crack path. The beam is notched with a 1 mm deep cut using a 60 degree blade at midspan to ensure predictable crack propagation path. The dimensions of the beam are 226 mm in length, 3.175 thick, and 25.4 mm width. The beam is loaded in the material testing machine for fatigue cycling.

Procedure: The method of Impedance spectroscopy is used to detect crack initiation and growth. The beam is fatigued at 10 Hz with a stress range of 57 MPa. The test was performed twice with impedance measurements taken under two loading schemes. One test took impedance measurements while the specimen was under a static axial load. The other test took measurements while the specimen was under sinusoidal axial loading. The specimen was never removed from the machine during the test. This ensures consistent boundary conditions throughout the test. A plot of the overlaid impedance measurements is given below. Impedance was measured from 30 to 110 KHz with a resolution of 20 Hz.

Results under static loading: A total of 36 impedance measurements were taken during the fatigue test. For the measurements taken in this experiment the MTS loading was shut off and

the measurements were taken with a 20 pound static load on the beam. The experiment in the following section is conducted while the beam is under dynamic fatigue loading. The measurements were taken at baseline and damaged states. An overlaid graph of all of the measurements becomes too cluttered to be useful. For this reason, in figure 3.3.4, we have plotted the baseline measurement and the final damaged measurement of impedance spectrum. This plot shows peak shifting and attenuation which has occurred during the course of the experiment. The damage metric was calculated for each case of fatigue.

In figure 3.3.5 and 3.3.6 damage index is plotted against crack length. From this plot it is possible to see that the crack was detectable at a length of 1.7 mm. The damage is considered detectable as there is a noticeable jump in damage metric which denotes a significant change in impedance signature. In this experiment we were able to successfully detect crack initiation using the impedance method while the beam was under a static load of 20 pounds.

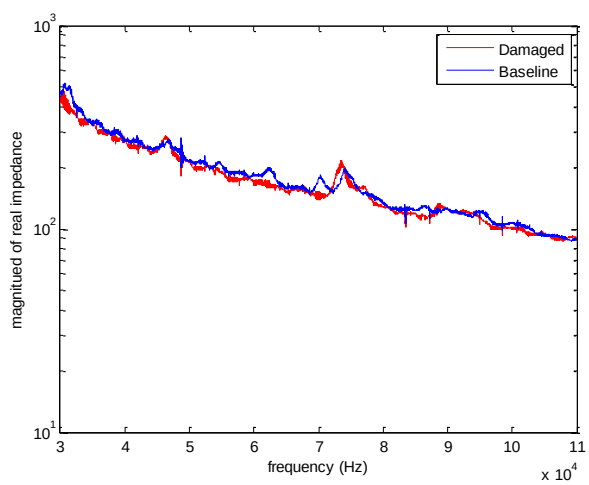

Figure 3.3. 4 Plot of baseline and damage impedance spectrum measurements for fatigue damage

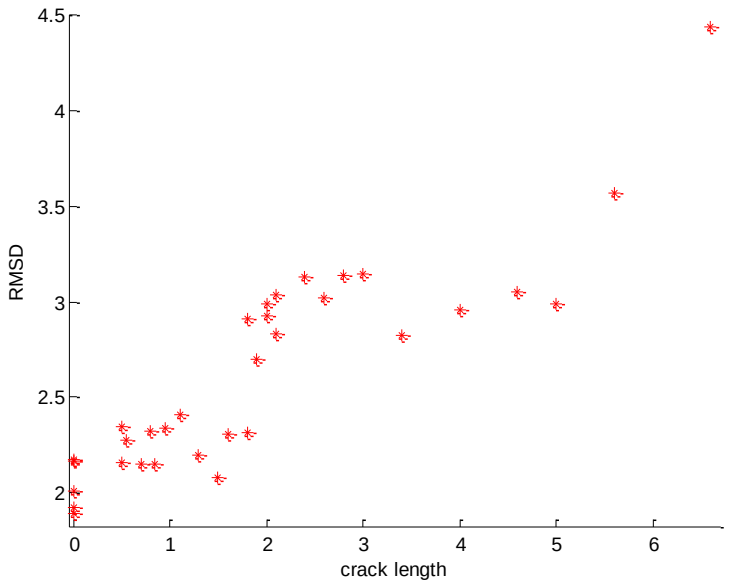

Figure 3.3. 5 Scatter plot of crack length vs. damage index for beam subjected to fatigue damage

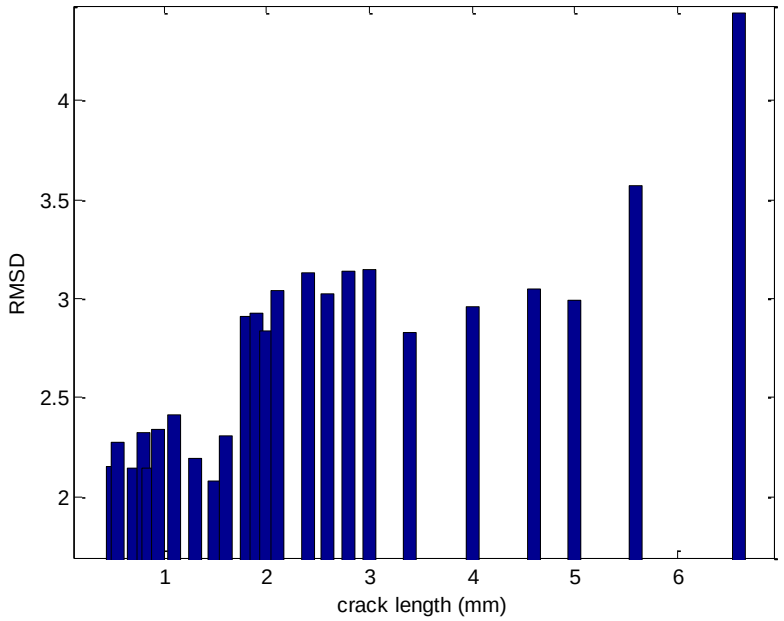

Figure 3.3. 6 Bar Graph of crack length vs. damage index for experimental beam

Results for Impedance of simple beam under dynamic load: The previous experiment took impedance measurements under a static load. Another experiment was conducted which took impedance measurements while the beam was being fatigued. The loading on the beam was sinusoidal axial loading at 20 Hz with a stress range of 57 MPa. The plot of RMSD damage index vs. crack length that was calculated for the dynamic load experiment is presented in figure 3.3.7. Damage index increases at a crack length of 1.6 mm. This is about the same size crack that was detectable when the measurements were taken under static axial loading.

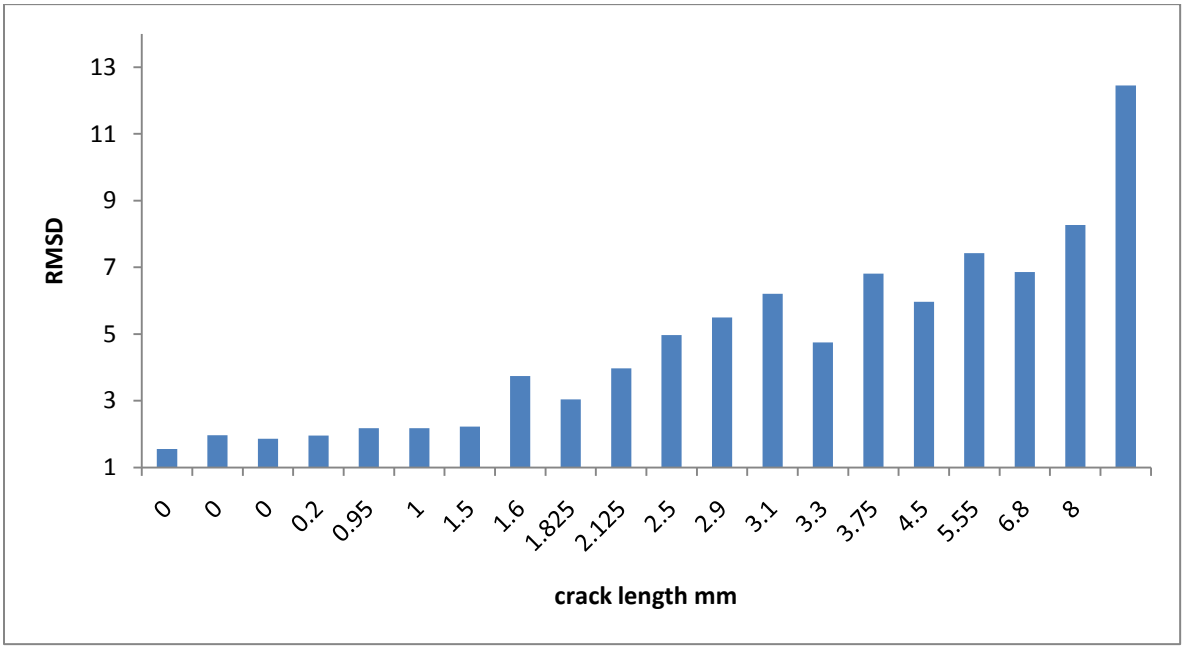

Figure 3.3. 7 Damage index vs. crack length for impedance measurements under dynamic load

Conclusions: The impedance method is effective at detecting fatigue damage in simple beams. The placement of the sensors is important for this method. Placing the sensor close to the crack path is necessary for detection. The impedance method can be used as a first indicator of damage as it is capable of detecting very small scale damage. It also can be concluded that the impedance method is effective even when the structure is under consistent operational loading.

Since similar size damages were detected under static axial loading and dynamic axial loading the impedance method has been shown to be attractive for in service SHM applications.

3.3.3 Impedance of Lug Joint under fatigue

Motivation: Since the impedance method is capable of detecting small scale fatigue damage on simple structures, it will be advantageous to extend this method to fatigue damage on a more complex specimen. The specimen considered here is a "Lug Joint" from the wing spar of an aircraft. The part that will be fatigued is shown in figure 3.3.8.

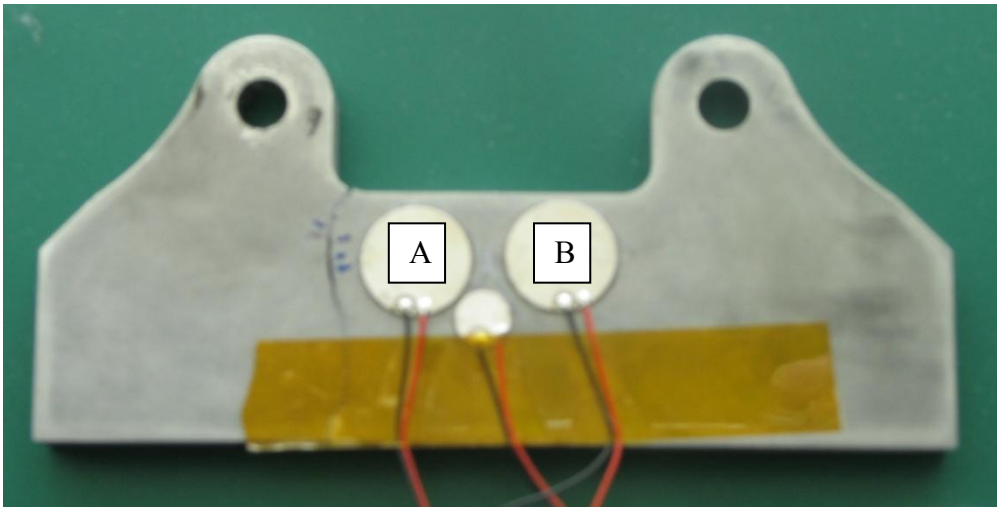

Figure 3.3. 8 Picture of lug joint used in fatigue experiment

Set Up: The lug joint is fitted with two round PZT patches. Since the part has two identical stress concentrations, it is not possible to predict which side of the lug will experience fatigue cracking first. For this reason a PZT wafer is placed near both stress concentrations. The PZT wafers are labeled A and B for clarity. The part is then loaded in the MTS machine using two clevises to simulate the boundary conditions experienced in the wing spar.

Procedure: The baseline impedance measurement is taken when the part is loaded in the MTS. The frequency spectrum measured is from 30K to 100K Hz with a resolution of 20Hz. The part is then subjected to fatigue loading from 110 pounds to 1100 pounds. This is a stress ratio of 0.1. The actuation was turned off every 50K cycles for impedance measurement until cracking occurred. The measurements were taken with the part under a 50 pound tensile load. Once cracking occurred, impedance measurements were taken every 2000 cycles.

Results: The crack initiated and grew at the stress concentration closest to PZT A at fatigued case 5. The size of damage at different fatigue cases is given in table 3.3.3. It was expected that the PZT closest to the crack would be most capable of detecting the fatigue damage. This did not turn out to be the case. PZT B showed a monotonically increasing damage index once damage occurred. PZT A was unable to show a satisfactory trend in damage index. In the future tests need to be conducted using a different shape PZT wafer. It has been found on numerous occasions that rectangular PZT wafers are capable of detecting small scale damage and even fatigue damage. It may be the shape, size, and location of the PZT that is confounding the results and making it difficult to detect damage on this specific specimen.

Table 3.3. 3 Damage size cracks at different number of cycles for impedance of lug joint

Fatigued Case	Number of Cycles	Crack length
1 (Baseline)	0	0
2	50k	0
3	100k	0
4	125k	0
5	175k	5mm
6	210k	6mm

7	213.5k	7mm
8	215.5k	8mm
9	217.5k	10mm

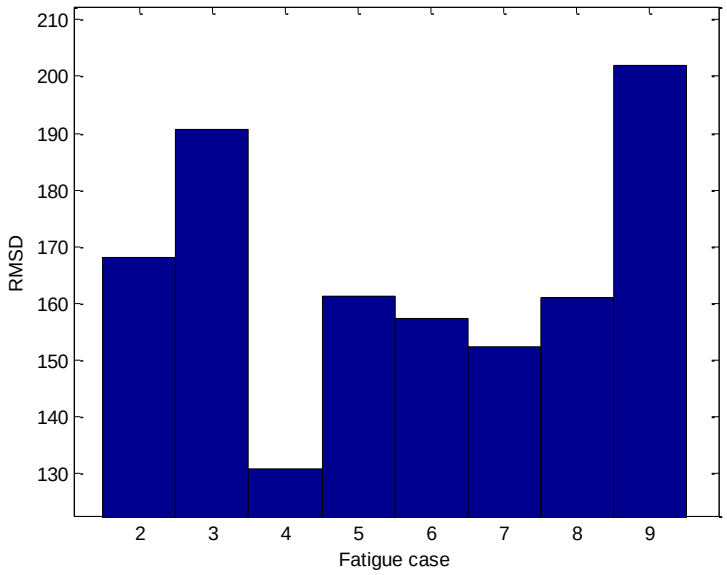

Figure 3.3. 9 RMSD damage index from PZT A impedance measurements

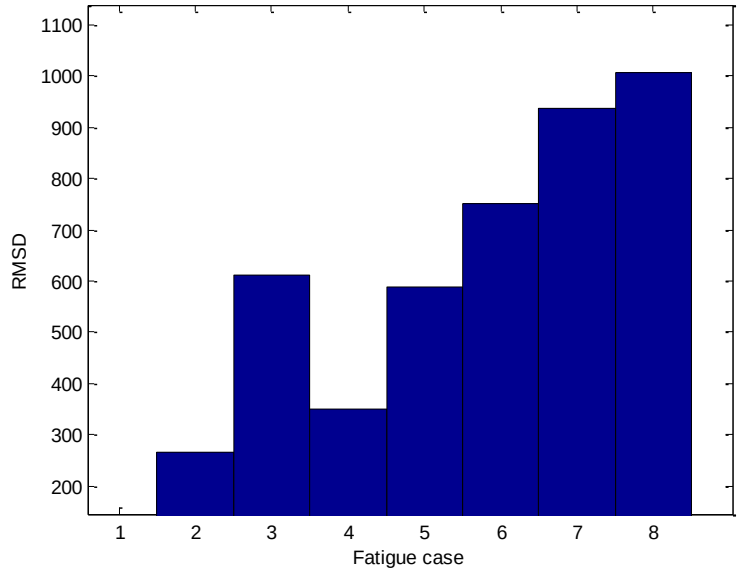

Figure 3.3. 10 RMSD damage index from PZT B impedance measurements

Conclusions: From this experiment it has been found that fatigue damage can be detected on a more complex specimen. When using circular PZT wafers the placement of the PZT is important, however, it is not necessarily the PZT with the greatest proximity to the cracking that will be best at detecting damage. Further experiments will be necessary to determine whether rectangular PZT wafers will be more effective at detecting damage.

3.4 Beat Method

3.4.1 Cantilever Beam Saw Cut Damage

Motivation: The beat phenomenon occurs when two signals that are close in frequency are subtracted from each other in the time domain. This effect is known to amplify the small difference in frequency. It has been determined analytically that this method will be able to

detect smaller shifts in frequency than the frequency domain method. Experiments have been designed to test the theory.

Set up: An experiment has been designed to test a proposed improvement to SHM using natural frequency shifts in the frequency domain. The proposed method uses the phenomena of beating caused by the subtraction of two signals with slightly different frequencies. The boundary conditions are cantilever and the dimensions of the beam are the same as in the saw cut experiment for natural frequency measurements. The structure is excited using an impact hammer to establish the free decay response of the beam. By using free decay signals we can obtain more information than exclusively doing the analysis in the frequency domain. The free decay signals can provide us with a beating damage metric as well as frequency domain damage metric. By performing a fast Fourier transform on the free decay signal of the beam it is possible to visualize the natural frequencies of the beam. The signal is recorded using a laser-vibrometer and SigLab. The mode of damage will be a saw cut 1.5 cm from the base of the beam. Although hammer excitation is used in this experiment as a proof of concept, an SHM system uses two PZTs. One is used for actuation and the other for sensing. The actuator vibrates at a frequency near the natural frequency of the beam. The actuation is then shut off and the resulting free decay is measured. Using this method no human interaction is needed. The procedure used in this analysis is used as a proof of concept for the improvement of sight of the beat method over direct natural frequency measurements.

Procedure: The SigLab is set to trigger as soon as the beam begins vibrating. The delay was set to -1 seconds. The sample rate was 390.6 microseconds/sample. The record length was 8192 samples. The beam was then struck with an impact hammer and the resulting decay signal was recorded. The free decay signals of damaged cases are first normalized to maximum amplitude

of one, the absolute value is taken, and then the damaged signal is compared with a baseline signal by subtracting the two signals. When the natural frequencies of the beam shift, the subtraction of the two signals will result in the beat phenomena, which will yield a damage metric of the period of the beat. Beating is predicted to occur at a frequency shift of 0.4% according to Cattarius (2000). Since the undamaged natural frequency is found at 67.8 hertz a shift of 0.2712 hertz should cause a beating in time. Damage is induced using the mode of a saw cut at levels of 0.23, 0.4, 0.9, 1.04, 1.46, 2.0, 2.46, and 3.0 mm.

Results: A plot of the undamaged free decay signal is given in figure 3.4.1. The damaged signals are subtracted from the healthy signal to produce a definite beating in time. Plots of the resulting signals are given in figures 3.4.2-3.4.7. From the analysis it was found that beating will occur at the second level of damage. This is a saw cut of 0.4 mm or 8% of the way through the beam. This shows improvement over the method of using natural frequency shifts directly. The method may be improved through more precise starting time of signals. If the start of the free decay signal is slightly shifted, the beating phenomenon may be confounded.

The frequency response function of the beam can also be established using these free decay signals. By doing a fast Fourier transform on the free decay signal, the dominant frequencies of vibration can be visualized. This results in an SHM method that uses one type of measurement and two damage detection algorithms. This would provide a more robust system than using just one damage detection algorithm.

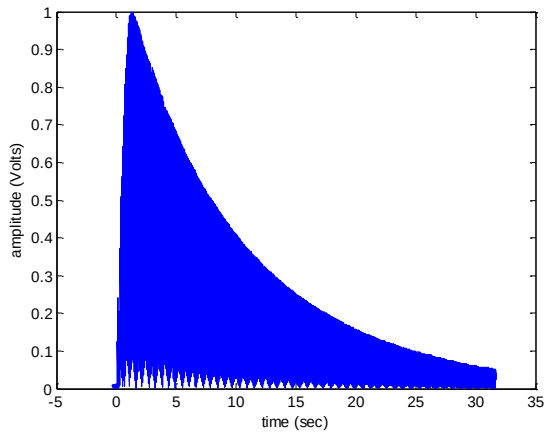

Figure 3.4. 1 Saw cut beat experiment (Free decay signal of baseline case)

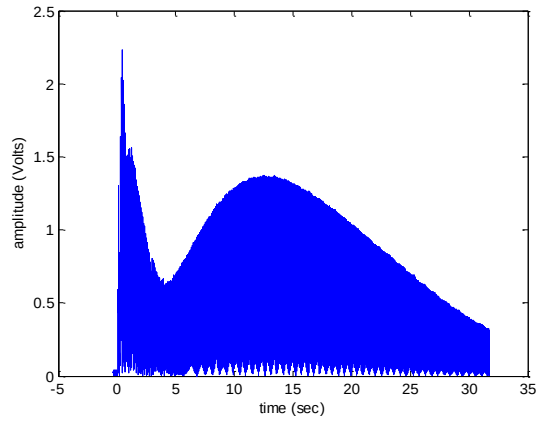

Figure 3.4. 2 Saw cut beat experiment (baseline minus damage case 1)

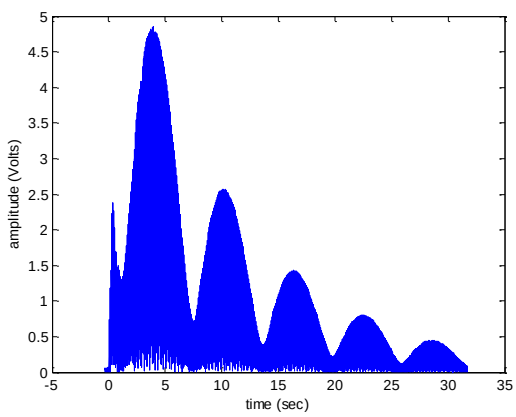

Figure 3.4. 3 Saw cut beat experiment (baseline minus damage case 2)

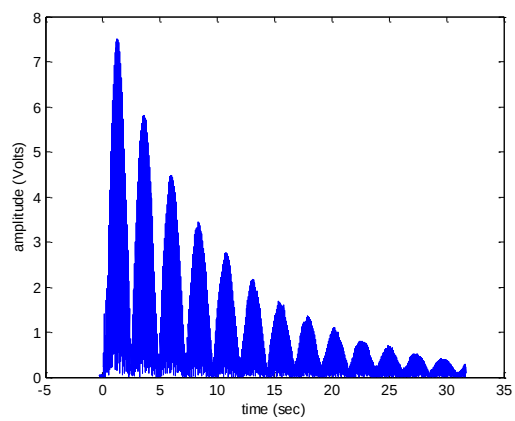

Figure 3.4. 4 Saw cut beat experiment (baseline minus damage case 3)

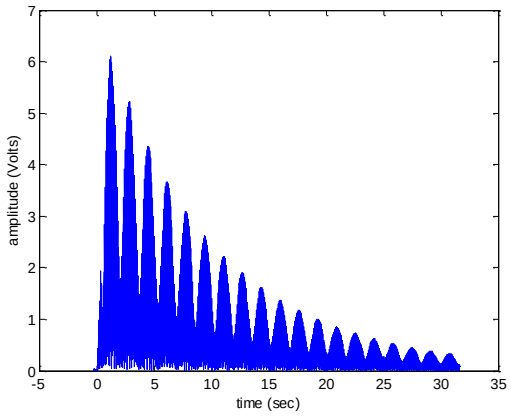

Figure 3.4. 5 Saw cut beat experiment (baseline minus damage case 4)

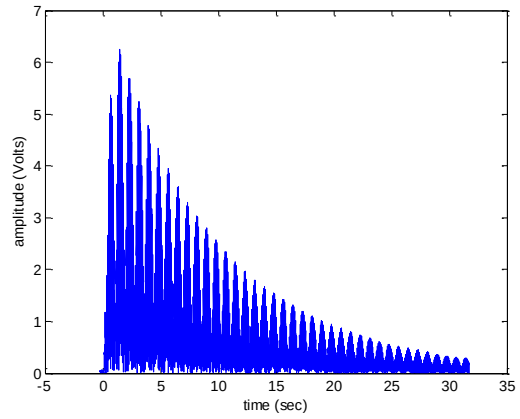

Figure 3.4. 6 Saw cut beat experiment (baseline minus damage case 5)

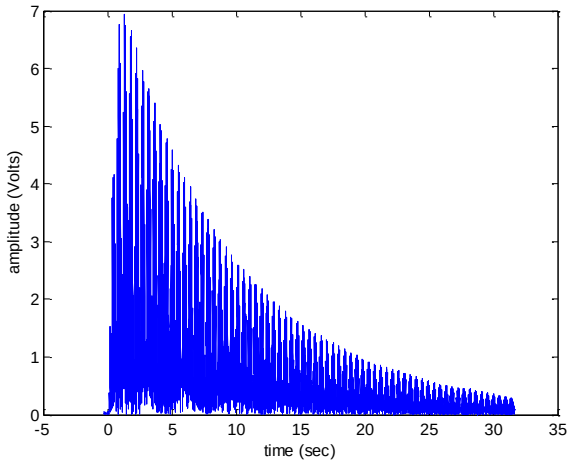

Figure 3.4. 7 Saw cut beat experiment (baseline minus damage case 7)

Conclusions

The measurement of free decay signals has been shown to be an improvement over the measurement of the frequency spectrum directly: however, the impedance method is still capable of detecting much smaller damage. The beating from the subtraction of two signals that are

close in frequency will amplify the small differences in frequencies. This will result in the ability to detect smaller damage than in the frequency domain. Using free decay signals is also advantageous as the frequency spectrum can be easily obtained using these signals. By simply taking the Fourier transform of the free decay signal we can establish the frequency response function. This results in the ability to use two damage detection algorithms using the same measurement.

3.4.2 Lug Joint undergoing fatigue cycling

Motivation: Since the beat method is capable of detecting smaller saw cut damage than the natural frequency method can detect on its own, the method is now applied to a more complex specimen.

Set up: The lug joint is loaded in the MTS machine for fatigue cycling. A picture of a lug joint is given in Figure 3.3.8. The lug is constrained fully in the clevises to minimize shifting. This is done by filling the extra space using washers. A picture of the lug constrained in the MTS machine is given in figure 3.4.8. The SigLab measurement system will be used to record the free decay signal due to hammer strike. These measurements will be used to evaluate natural frequency shifts during fatigue cycling.

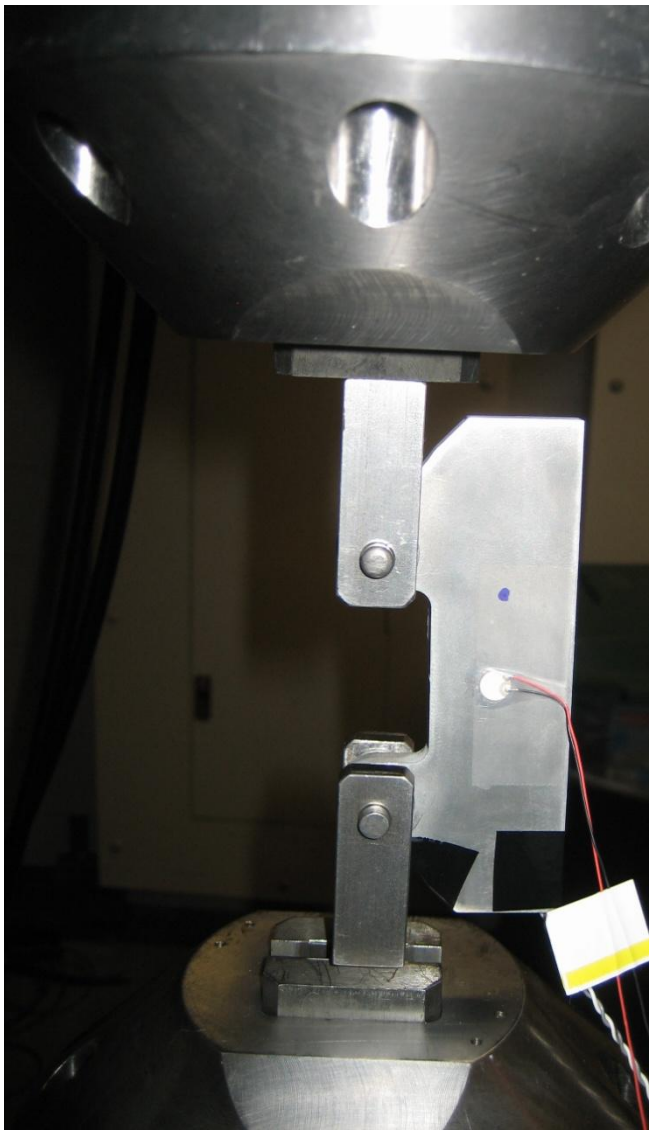

Figure 3.4. 8 Lug Joint Constrained in MTS machine

Procedure: Fatigue cracking was introduced in a lug specimen using cyclic loading from 110-1100 pounds. This is a stress ratio of 0.1. The beam was monitored for cracking by eye as well with the assistance of a magnifying glass. The beam was excited with an impact hammer, while contained in the test grips under a 50 lb tensile load. The resulting free decay signal from the

PZT sensor was recorded using VOS mode in SigLab. This was done at an undamaged state as well as in multiple fatigued states.

The decay signals were normalized to a magnitude of one and the absolute value was taken. Once this was accomplished the signals from the samples which had undergone fatigue cycles were subtracted from the baseline signal

Results: A table of how the crack grows with fatigue cycling is given in table 3.4.1. The resulting subtracted signals from the fatigue test are presented in Figures 3.4.9 through 3.4.18. By taking the Fourier Transform of the decay signal we can obtain the frequency spectrum of the lug. A sample spectrum is given in Figure 3.4.19.

From the subtracted signals we can see that a distinct beating occurs once damage is initiated. The period of the beat decreases with increasing damage. This is to be expected as the natural frequency shifts further from the baseline frequency. Although it seems that beating may occur at the lower cycles with no cracking, distinct beating occurs when the crack is between 3 and 5.5 mm.

Through the use of Fourier transforms the natural frequency of the lug was tracked during cracking. The frequencies are presented in Table 3.4.1. From this data it is very difficult to distinguish damage. Natural frequencies shift throughout the course of the experiment.

Conclusions: The beat frequency method was capable of detecting a fatigue crack of less than 5.5 mm. It was found that the natural frequency method was not able to successfully detect the damage although the beat method was able to. This leads us to believe that the beat method may also be more capable of avoiding false alarm damage than the natural frequency method. Not only is this method capable of finding smaller damage than the natural frequency method, it is

also less sensitive to false alarm damage when considering parts that are susceptible to fatigue cracking in an environment with ambient vibrations.

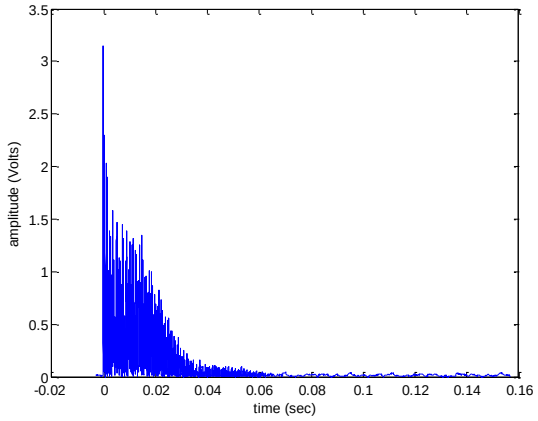

Figure 3.4. 9 Lug joint Fatigue Beat test (Baseline minus 30k cycle signal)

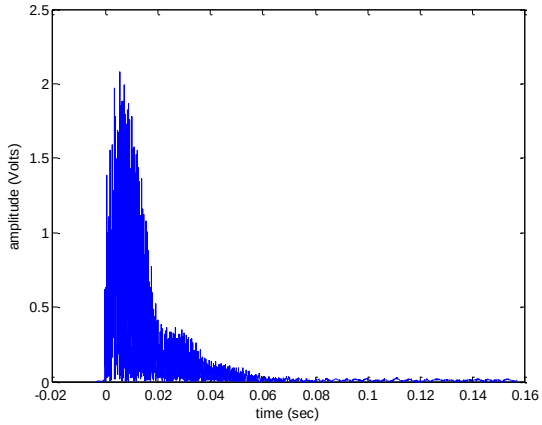

Figure 3.4. 10 Lug joint Fatigue Beat test (Baseline minus 60k cycle signal)

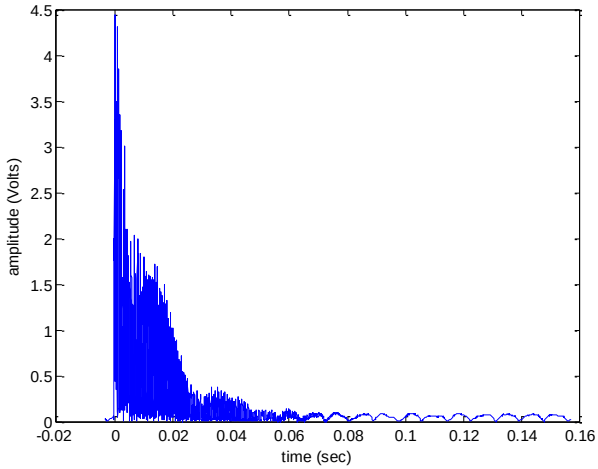

Figure 3.4. 11 Lug joint Fatigue Beat test (Baseline minus 90k cycle signal)

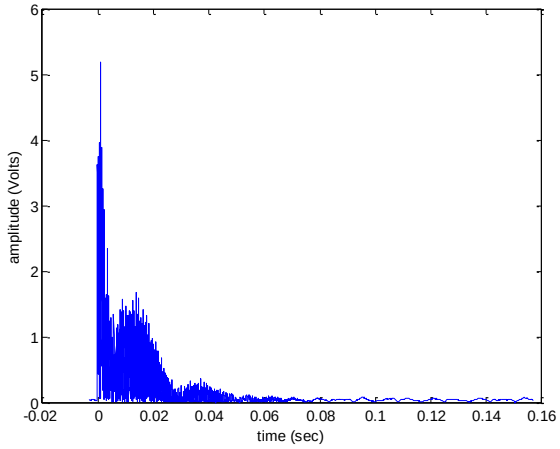

Figure 3.4. 12 Lug joint Fatigue Beat test (Baseline minus 120k cycle signal)

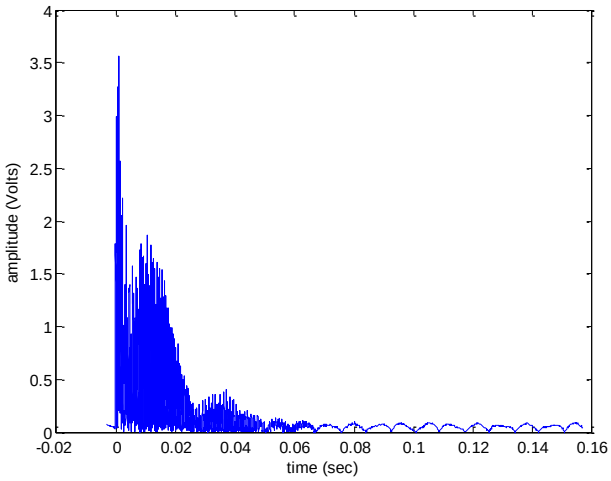

Figure 3.4. 13 Lug joint Fatigue Beat test (Baseline minus 150k cycle signal)

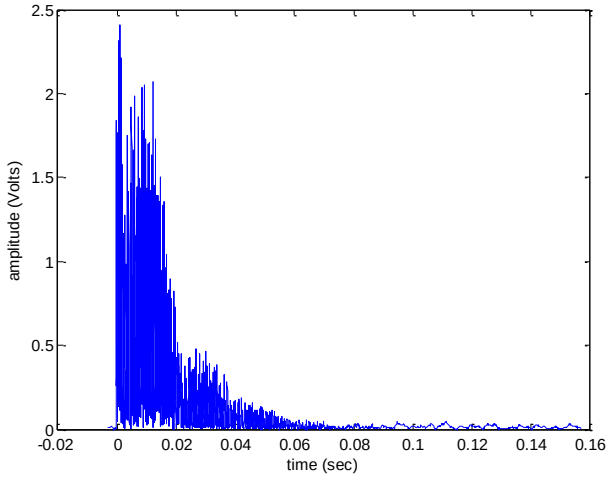

Figure 3.4. 14 Lug joint Fatigue Beat test (Baseline minus 180k cycle signal)

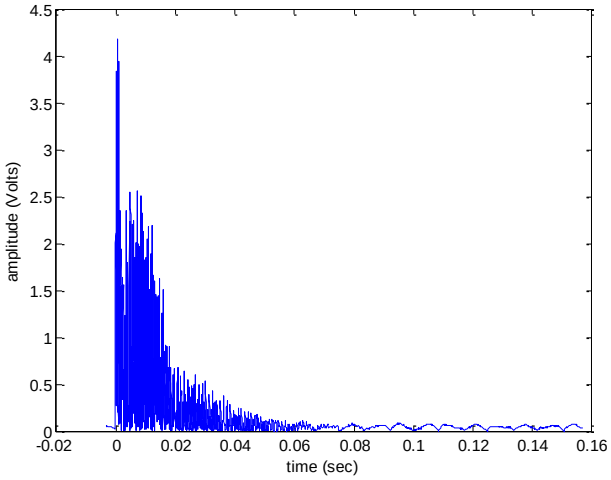

Figure 3.4. 15 Lug joint Fatigue Beat test (Baseline minus 190k cycle signal)

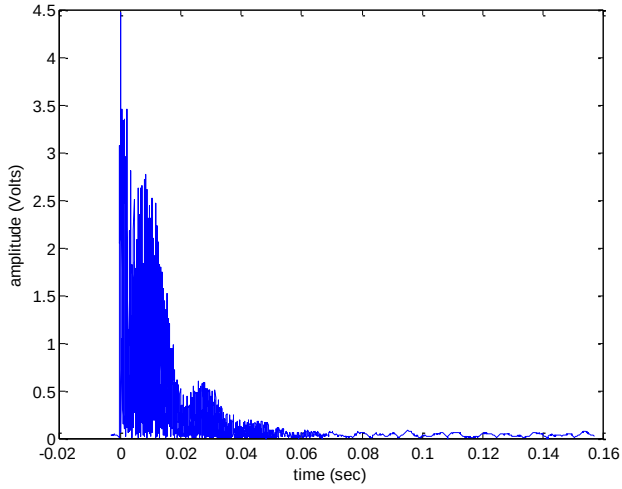

Figure 3.4. 16 Lug joint Fatigue Beat test (Baseline minus 193k cycle signal)

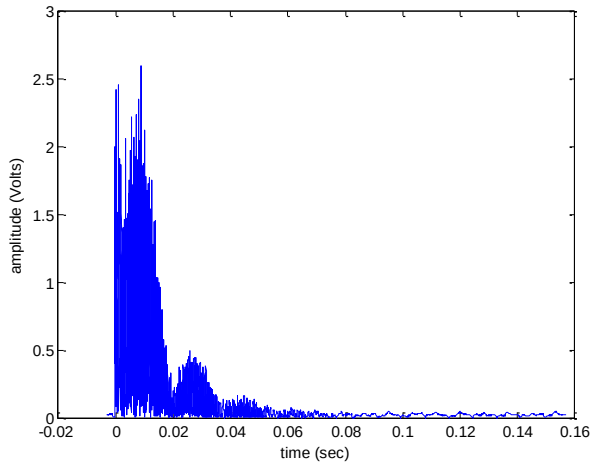

Figure 3.4. 17 Lug joint Fatigue Beat test (Baseline minus 196k cycle signal)

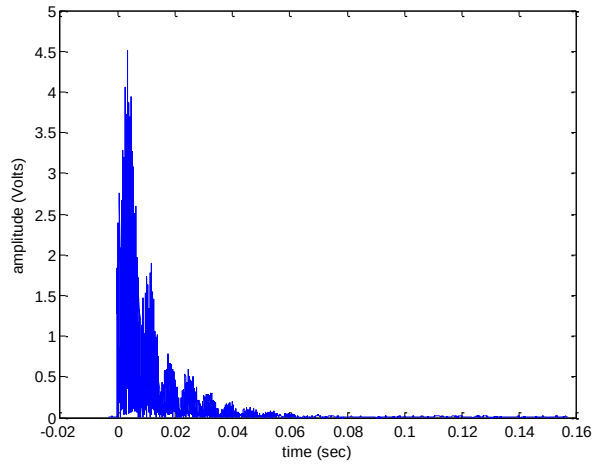

Figure 3.4. 18 Lug joint Fatigue Beat test (Baseline minus 198k cycle signal)

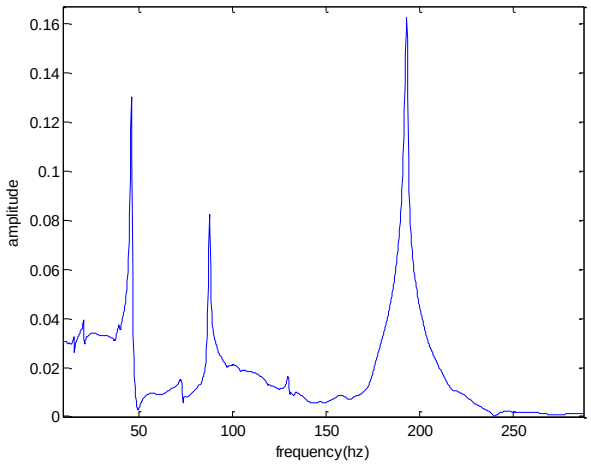

Figure 3.4. 19 Sample frequency spectrum oubtained through Fourier analysis of free decay signal

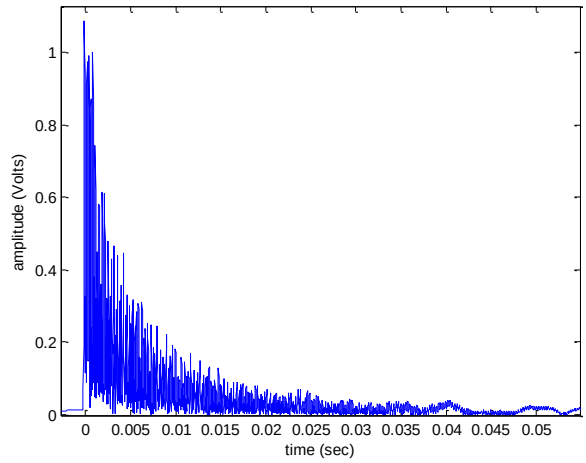

Figure 3.4. 20 Sample Decay signal graph after normalization and absolute value

Table 3.4. 1: Natural Frequency Data and Crack length vs. cycles data for lug joint beat experiment

Cycles	Crack length	ω1	ω2	ω3
0	0	47.4	90	195.4
30k	0	46.1	87.2	194.2
60k	0	45.8	85.9	192.9
90k	0	45.8	90.4	193.8
120k	0	45.8	90.1	193.8
150k	0	45.8	89.4	193.8
180k	0	45.8	87.8	193.2
190k	3 mm	45.8	87.5	192.9
193k	5.5 mm	45.5	88.8	192.9
196k	7 mm	45.5	90.4	192.9
198k	11 mm	44.9	85.6	188.4

3.5 Direct measurement of Stress Intensity factor using MFC sensors

Motivation: Yukio Fujimoto (2003) has shown that it is possible to measure stress intensity factors directly using monolithic piezoelectric material; however, this raw PZT is brittle and labor intensive to ~~cut to~~ ~~(~~prepare~~?)~~ usable sizes. In addition, monolithic piezoelectric materials may have an issue with the lack of durability. In other words, monolithic piezoelectric sensors are more vulnerable to fatigue damage than structures in some cases.

On the other hand, macro fiber composites can simplify use because of their unique packaging which allows them to be pre-sized and more robust. Macro fiber composite patches are made up of small Piezo-ceramic fibers that are interwoven with electrodes. The active area is then layered between adhesive and a durable polyamide film Material (2010). This type of sensor is a more attractive candidate for applied SHM systems due to its proven durability, convenience, and larger coupling coefficient. The voltage output of MFC is also higher which will lead to a better signal to noise ratio.

Experimental Set Up: A beam of Al-6061 is prepared for a validation of the direct measurement of stress intensity factors using MFC patches. The yield and tensile strengths of the aluminum beam are 241 MPa and 290 MPa, respectively. The dimensions of the beam are the same as in the theoretical calculations in section 2.5. The beam is notched for crack propagation at midspan. The notch is one millimeter deep and is ~~made~~ fabricated with a 60 degree saw blade. This is used to create a stress concentration to ensure a predictable location of fatigue crack initiation.

The beam is prepared using MFC patches. ~~The patches are ordered from Smart Material.(removed to avoid any commercial The model is M2814 P1.~~ The dimension and the piezoelectric properties of the MFC are summarized in Table 3.5.1.

Table 3.5. 1: Properties and dimensions on MFC Patches used in SIF experiment

Overall Dimensions	37mm x 17 mm
Active Area	28 mm x14 mm
IDE Spacing	0.5 mm
Capacitance	1.2 nF

PZT Type	Navy Type II
Max Voltage	-500v to +1500 V
Max Tensile Strain	4500 ppm
Thickness	0.3 mm

The two sensors come sized for our experimental beam and are ready to be adhered to the metal specimen. The active area of the MFC patch is considered to be the area which contains the piezoelectric fibers. The MFC patches are adhered on either side of the crack propagation path. The distance from the active area of the MFC to the crack propagation path is 3 mm. This distance is known as H_0 in the Fujimoto (2003) paper. They are adhered using a vacuum packing procedure with the adhesive being epoxy resin. Once the resin has set we can solder leads of a twisted pair of wires to the positive and negative terminals of the MFC. The specimen is now ready for axial loading and calibration. A picture of the experimental beam with attached MFC patches is given in Figure 3.5.1.

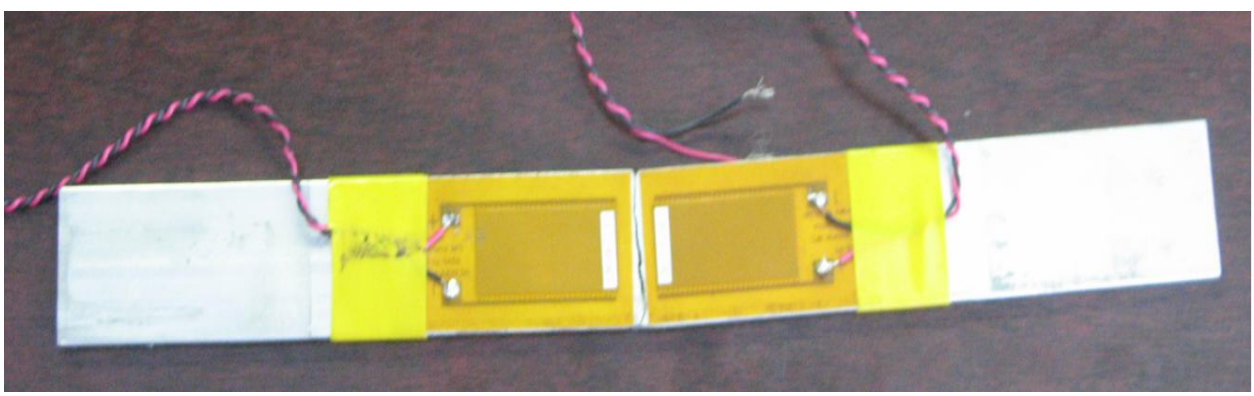

Figure 3.5. 1Picture of experimental beam after brittle fracture

The specimen is next loaded in the MTS machine. It must be ensured that the specimen is square in the machine in order to achieve true axial loading. The specimen is loaded under a cyclic fatigue loading at stress ratio of 0.1. The positive and negative leads of both sensors are wired to a 2-channel digital oscilloscope. The oscilloscope is equipped with USB output to a laptop computer. Using this interface it is possible to store waveform data, time series data, and measurement data (such as Peak to Peak voltage). A picture of our experimental set up is given in Figure 3.5.2.

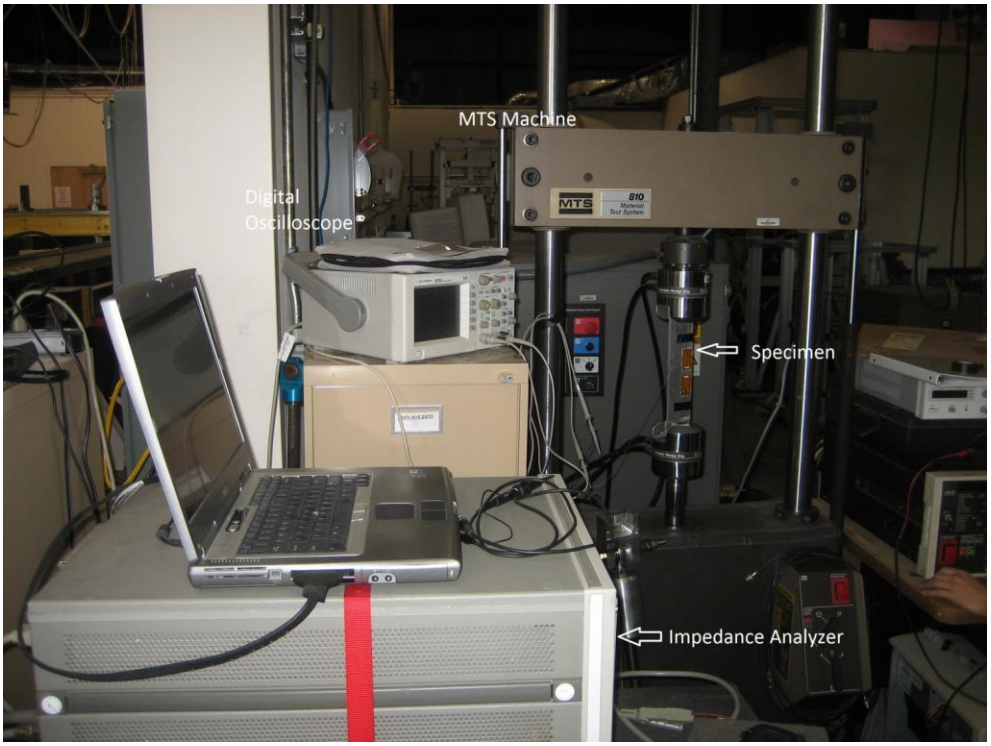

Figure 3.5. 2 Picture of experimental set up showing instrumentation

Procedure

Calibration of Voltage to Stress for SIF Test: The sensors must first be calibrated in order to obtain a constant of proportionality parameter by applying a known stress range and measuring the output voltage of the MFC using the digital oscilloscope. The constant varies depending on

the type of MFC as well as adhesion condition. -The parameter of interest is the peak to peak voltage at the given stress range. ~~This must be done for both the MFC specimen and the bare PZT specimen.~~ The equation for calculation of the calibration constant is,

$$C = \frac{V}{\sigma * S} \qquad 3.5.1$$

In this equation V is the peak to peak voltage output of the MFC. Here, σ is the stress range and S is the active surface area of the MFC. The area considered active can be seen in figure 3.5.3. In the y dimension the entire height H is active. In the x dimension only the width of the MFC after the crack is active. For an undamaged beam the entire width is active, however, as the crack grows the stress field will change and will decrease the amount of MFC that is being stressed. The parameter $L2$ in figure 3.5.3 describes the active width of the MFC that is being stressed as the crack grows.

By applying a series of known stress amplitudes and monitoring the output voltage of the patches we obtain an average calibration constant for the given sensor-bond relationship. This calibration constant is used in the ~~calculation~~ measurement of the stress intensity factor. Multiple tests are conducted at different stress amplitudes to ensure the consistency of the calibration coefficient.

Fatigue test measurement of SIF: Once the sensors have been calibrated the specimen ~~must be~~is exposed to a cyclic ~~fatigued~~ fatigue loading to induce a fatigue crack. The specimen is loaded in force control~~rol~~ with a stress range of 57 MPa with a stress ratio of 0.1 ~~from 500 to 1500 pounds (need to change to Newton? As most journal use SI units.)~~ at a frequency of 10 Hz. ~~This corresponds to a stress range of 57 Mpa.~~ A counter is enabled to provide the number of elapsed fatigue cycles. The fatigue crack initiation and fatigue crack propagation are monitored by eye with the aid of a magnifying glass.

The peak to peak voltage output of both MFC patches is recorded using the digital oscilloscope before cracking occurs and during crack growth. During crack growth the crack tip location is marked on the specimen and labeled with the corresponding number of cycles for later measurement. The output voltages will be later used for direct calculation of the Stress Intensity factor.

Calculation of SIF from measured voltage: Using the method of Fujimoto (2003) we can convert our voltage measurements to stress intensity factors. The voltage output of a MFC sensor is proportional to the stress applied. The relationship between stress and voltage for monolithic PZT is

$$V = C * k \int (\sigma_x + \sigma_y) dS \qquad 3.5.2$$

Here *C* is the experimental calibration constant obtained in advance in the calibration stage, *k* is the stress state constant. For plane stress *k* is equal to 1 and 0.~~73~~ 74 for plane strain which is given in elasticity theory. The active surface area of the MFC is *S*. It should be noted that for an MFC the stress in the y direction may not contribute to the voltage ouput due to the isotropic properties of the MFC. The stress intensity factors for mode 1 (*Ki*) and mode 2 (*Kii*) are given by

$$Ki = \frac{V1+V2}{2*C*k*G1} \qquad 3.5.3$$

and

$$Kii = \frac{V2-V1}{2*C*k*G2} \qquad 3.5.4$$

V1 and *V2* are the output voltages measured from the MFC patches. *G1* and *G2* are computed from

$$G1 = \int_{H_0}^{H_0+H} \int_0^{L_2} \sqrt{\frac{\sqrt{x^2+y^2}+x}{\pi(x^2+y^2)}} dxdy \qquad 3.5.5$$

$$G2 = \int_{H_0}^{H_0+H} \int_0^{L_2} \sqrt{\frac{\sqrt{x^2+y^2}-x}{\pi(x^2+y^2)}}\, dxdy \qquad 3.5.6$$

It may be noted that the limits of integration are slightly different from those derived in the paper by Fujimoto. In Yukio Fujimoto (2003) the limits of integration in the *x* dimension for *G1* and *G2* are *–L1* to *L2*. This equation is to be integrated over the surface area of the Piezo-electric. For our geometry the active surface area of the MFC that is under stress will change with crack length. When considering these limits of integration the integration domain stays relatively constant. As *L1* grows, *L2* decreases. The distance in the *x* dimension that is stressed is from the crack tip to *L2*. If we consider the origin to be the crack tip, we can integrate from 0 to *L2*. As the crack grows the integration domain will decrease as less of the area of the MFC is under stress. The limits of integration being from *L1* to *L1+L2* also provide satisfactory results. This is considering the left edge of the beam to be the origin. In this experiment, the values of H_0 and *H* are 3mm and 24 mm, respectively. *L2* varies with crack length. The geometry is shown in figure 3.5.3. Using the altered limits of integration it was found that the experimental data had a much better fit to the analytic solution.

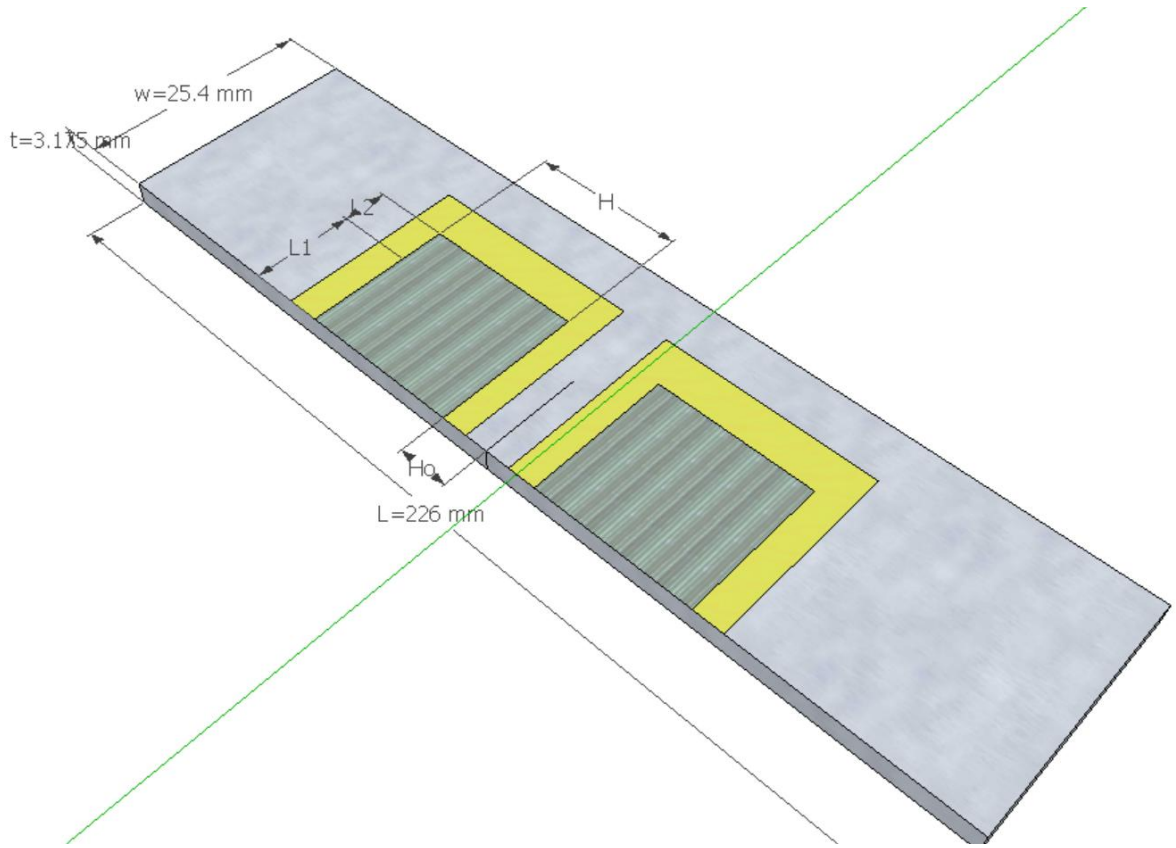

Figure 3.5. 3 Beam Geometry and MFC placement for measurement of Stress intensity factors

Results

Calibration: A calibration coefficient was calculated for different stress ranges and both MFC patches. The data used to calculate the coefficients is given in Table 3.5.2 . An average *C* value of *0.002* and was found to be consistent for multiple experiments using the same style MFC sensor.

Table 3.5. 2: Table of output voltages at different stress ranges for calculation of calibration constant for SIF test

Stress Range	force range N	Va	Vb	Cal Constant a	Cal Constant b
40.1774856	3113.75513	31.4	27.4	0.002325989	0.002029684
45.9171264	3558.5773	34.6	30.8	0.002242653	0.00199635
51.6567672	4003.39946	36.6	34.2	0.002108699	0.001970424
51.6567672	4003.39946	35.6	33.8	0.002051084	0.001947378

Fatigue Test

Once the MFC patches were calibrated, the beam is cycled for fatigue. The beam is subjected to sinusoidal axial loading at 10 ~~hz~~ Hz with a 57 MPa peak to peak stress range. It took almost 200 thousand cycles for the crack to initiate. In order to induce cracking sooner, a higher load could have been used; However for our experiment, we wished to have a somewhat slow crack growth in order to get many SIF measurements. A plot of crack length vs. number of cycles is given in figure 3.5.4.

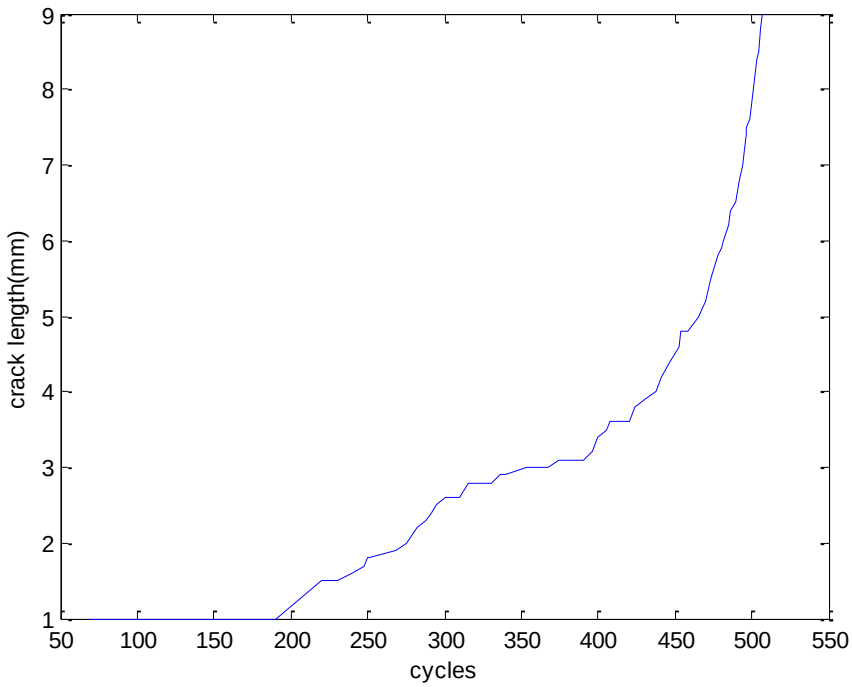

Figure 3.5. 4 Plot of crack length vs. number of cycles

Throughout the course of the experiment the peak to peak voltage output of both MFC patches are recorded. A plot of voltage vs. crack length is given in Figure 3.5.5.

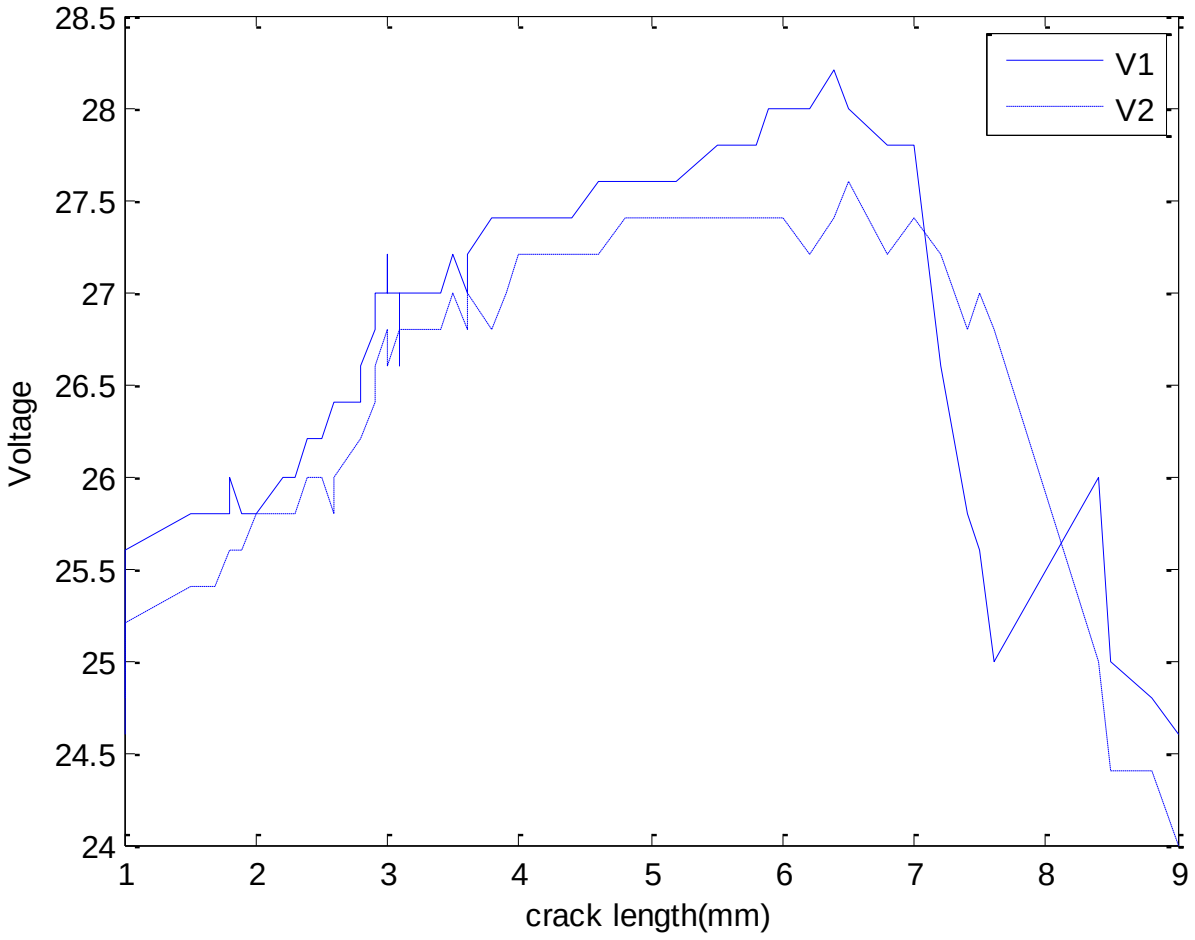

Figure 3.5. 5 Plot of voltages vs. crack length for first experiment

We can see from figure 3.5.5 that voltage increases when the crack initiates and grows until the crack becomes about 6 mm in length. At this length, which is 40 percent of the width of the MFC, the voltage begins to drop off rapidly. This phenomenon may be useful in other crack detection algorithms. These voltage measurements are used with equations 3.5.3 and 3.5.4 to predict *Ki* and *Kii* stress intensity factors. This experiment was carried out twice and the SIF

data for both experiments are presented below. Plots of ~~*K1*~~ *Ki* and ~~*K2*~~ *Kii* SIF vs. crack length for both experimental and theoretical data are presented in Figures 3.5.6 and 3.5.7.

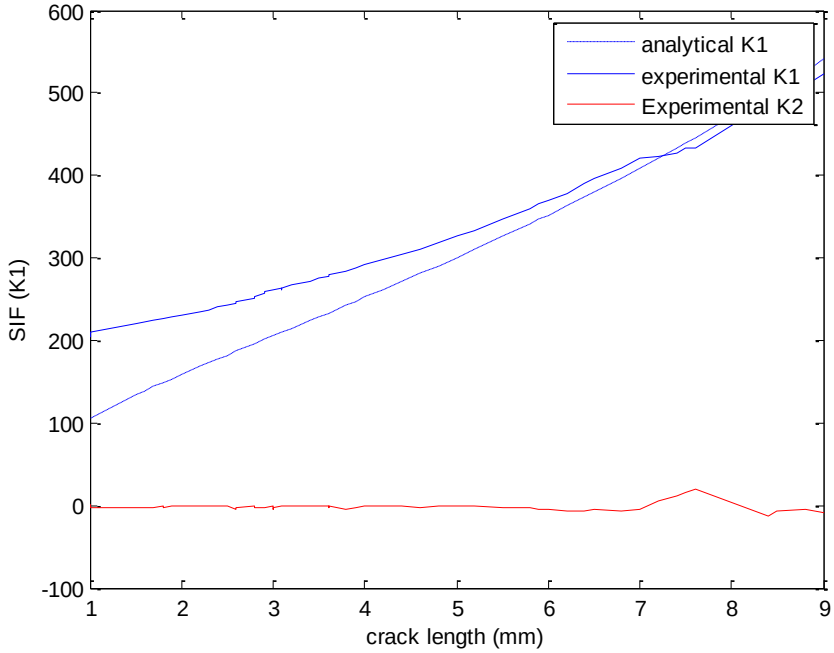

Figure 3.5. 6 Comparison between analytical and experimental stress intensity factors 1st experiment

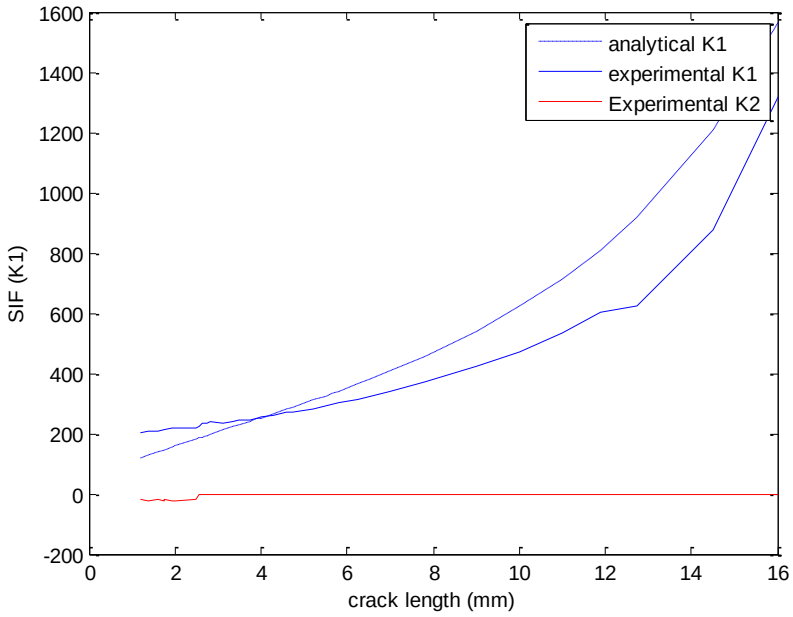

Figure 3.5. 7 Comparison between analytical and experimental stress intensity factors 2nd experiment

These plots show that a high level of agreement exists between the predicted and measured SIF values. A maximum of 19% error exists when the crack is very small. Although this is a high level of error, the error decreases as the crack grows. A plot of *Ki* SIF vs. length agrees well with the predicted values. The error is calculated for the 1st experiment and is plotted in figure 3.5.8. The error is at its maximum when the crack first initiates. As the crack grows the SIF measurement has decreasing error. *Kii* is predicted to be 0 for all levels of cracking in the plane stress configuration. More effort should be spent determining why the error is high when the crack is small.

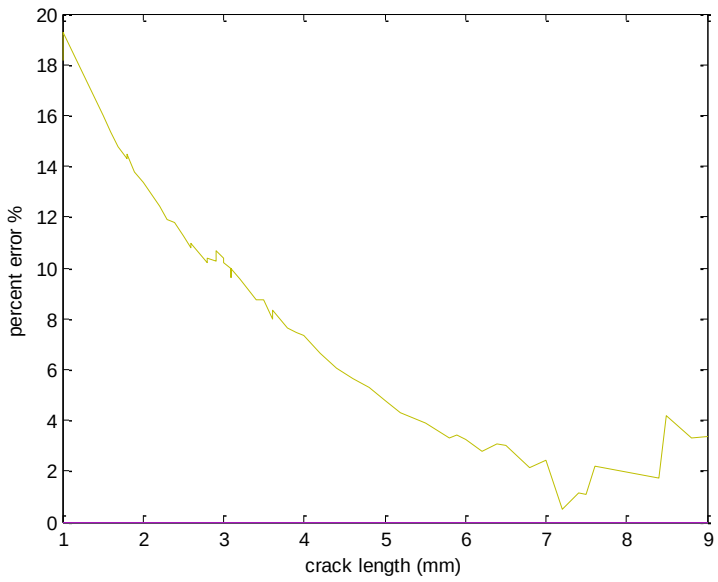

Figure 3.5. 8 Percent Error vs. crack length for first SIF experiment

Conclusions and Recommendations

It is possible to determine the severity of damage at different crack lengths by directly measuring the SIF of the crack. This method may be useful in developing an integrated SHM system for hotspots. Stress intensity factors are important parameters necessary for predicting remaining fatigue life and have so far been difficult to measure accurately for structures with complex geometry. With the information that this method provides, it may be possible to extend the service life of structures. One remaining issue with this method is that the measurement is somewhat inaccurate at low levels of cracking.

Another advantage of monitoring the voltage of MFCs under load is that it can provide multiple damage indicators for an SHM system. Although using the voltages for SIF measurements is an NDE system, the data acquisition can be used for SHM. The voltage plot shown in figure 3.5.5 has some distinct features that can be attributed to damage if the structure is under sinusoidal

loading. First, the voltage will increase almost immediately when a crack forms. This could be considered an indication that damage has occurred. Second, the voltage will drop off very quickly when the crack becomes 40% of the width of the MFC. By placing the MFC so that critical crack length corresponds to 40% of the width of the MFC, the voltage will begin to drop when the crack becomes critical. Voltage measurements could be very useful in an SHM system as the hardware required to collect them is relatively inexpensive and the data analysis is computationally inexpensive.

Chapter 4: Conclusions and Recommendations

The methods presented in this thesis can be used to monitor hotspots on structures. The methods presented include the monitoring of natural frequencies using burst-chirp signals in the frequency domain, monitoring of free decay signals in the time domain to establish a beat phenomena via a subtraction method, impedance spectroscopy, and the direct measurement of stress intensity factors using macro-fiber composites.

Vibration methods were evaluated to determine the smallest crack that can be detected using frequency shifts. This is an important step in determining the feasibility of implementing these methods on real structures. It was found that using time series free decay signals can yield a more robust system of damage detection. For saw cut damage and fatigue damage the beat method shows a distinct advantage over frequency domain methods. Not only can the beat method detect smaller damage, but for the case of parts under fatigue, it may be less likely to produce false alarm damage. Both natural frequency methods can be confounded by ambient vibrations as well as changes in temperatures.

The impedance method was found to be capable of detecting much smaller cracks than the vibration methods. This was true for both saw cut damage as well as fatigue damage in simple beams and the more complex specimen of lug joint. This method is incredibly versatile and shows great promise as an SHM system that may be implemented in real structures. For this reason it is suggested that the impedance method be used in conjunction with the SIF method to provide a multifaceted monitoring technique for hotspots on structures under fatigue loading. More effort needs to be made to reduce the cost and size of the hardware required to measure the impedance spectrums. Also, effort should be spent in determining the effect of operational load on the impedance method.

A multifaceted approach to the monitoring of structures can be implemented by the specific sensor placement used in the SIF and impedance experiments. By placing MFC patches on either side of the predicted crack path, a rather useful detection algorithm can be implemented. The impedance method can be used as a first alarm for detecting damage due to its high sensitivity to cracking. By monitoring the voltage output of the MFC we can measure the severity of the crack by converting the voltages to stress intensity factors. In cases where the part is undergoing a consistent loading scheme, the voltage measurements may be able to provide a damage alarm as well. Since the voltage will increase as the damage occurs and rapidly decrease when it reaches a certain size, the voltage measurements can provide us with an additional damage metric. The algorithm for calculating stress intensity factors from voltage data has been improved during this effort. For our specific geometry the limits of integration on the *G1* and *G2* factors, which are used for calculating the *Ki* and *Kii* factors, needed to be modified to provide satisfactory results.

The state of the art has been expanded by this effort in a few ways. By implementing multiple monitoring methods on similar size specimens, a comparison between detectable crack sizes is possible. It has been shown that the impedance method is capable of detecting smaller damage than the vibration methods. It has also been demonstrated that the impedance method is effective when the host structure is under sinusoidal loading. Many methods of interrogation are only capable of detecting damage when the structure is not under load. The impedance method can detect damage under load almost as well as when the part is out of service. This makes the method very attractive for structural health monitoring. Conclusions have been drawn about the detectable crack size using vibration and impedance methods with respect to two different planes of damage. In-plane damage is more easily detected using the impedance method. In-plane and

out of plane damage are both detectable using vibration methods. Smaller cracks are detectable when the damage is in the same plane as the attachment of the PZT. MFC patches were shown to be effective at measuring stress intensity factors. Previously only monolithic PZT was used to do this. The algorithm used to calculate SIFs was also improved.

Further research should be conducted in applying the impedance/SIF method to more complex structures. Applying this method to weld joints would be especially useful, as the analytical solution for this is unreliable. Analysis should be conducted as to which structures the vibration methods would be most useful in monitoring. It would be interesting to extend the vibration methods to self excited structures. The impedance method shows great promise for application to real structures in an SHM system. The main issue facing this method is the size, weight, power consumption, and fragility of the hardware required to measure impedance signatures. Research should be conducted in developing a small form factor, low cost, and robust impedance analyzer.

Bibliography

Abdul-Aziz, A., J. J. Trudell, et al. (2006). Finite element design study of a bladed, flat rotating disk to simulate cracking in a typical turbine disk; part II. Nondestructive Evaluation and Health Monitoring of Aerospace Materials, Composites, and Civil Infrastructure V, San Diego, CA, USA, SPIE.

Anton, S. R., G. Park, et al. (2007). On piezoelectric Lamb wave-based structural health monitoring using instantaneous baseline measurements, San Diego, California, United States, SPIE.

Ashby, M. F. (1999). Materials Selection in Mechanical Design. Woburn, MA, Butterworth-Heinemann.

Aydin, K. (2008). "Vibratory characteristics of Euler-Bernoulli beams with an arbitrary number of cracks subjected to axial load." JVC/Journal of Vibration and Control **14**(4): 485-510.

Binici, B. (2005). "Vibration of beams with multiple open cracks subjected to axial force." Journal of Sound and Vibration **287**(1-2): 277-295.

Brandon, J. (2000). "Nonlinear vibration of cracked structures: Perspectives and horizons." Shock and Vibration Digest **32**(4): 273-280.

Carneiro, S. (2000). Model-Based Vibration Diagnostic of Cracked Beams in the Time Domain. Engineering Mechanics. Blacksburg, Virginia Tech. **PhD:** 165.

Cattarius, J. (1997). "Time Domain Analysis for Damage Detection in Smart Structures." Mechanical Systems and Signal Processing **11**(3): 409-423.

Cattarius, J. (2000). "Experimental verification of intelligent fault detection in rotor blades." International Journal of Systems Science **31**(11): 1375-1379.

Cawley, P. (1979). "The location of defects in structures from measurements of natural frequencies." The Journal of Strain Analysis for Engineering Design **14**(2): 49-57.

Chondros, T. G. and A. D. Dimarogonas (1980). "Identification of cracks in welded joints of complex structures." Journal of Sound and Vibration **69**(Copyright 1981, IEE): 531-538.

Chondros, T. G., A. D. Dimarogonas, et al. (1998). "Longitudinal vibration of a bar with a breathing crack." Engineering Fracture Mechanics **61**(5-6): 503-518.

Dimarogonas, A. D. (1996). "Vibration of cracked structures: A state of the art review." Engineering Fracture Mechanics **55**(5): 831-857.

Doebling, S. W., C. R. Farrar, et al. (1998). "Summary review of vibration-based damage identification methods." Shock and Vibration Digest **30**(2): 91-105.

Duan, Z.-D., G.-R. Yan, et al. (2008). "Challenges in applying the vibration-based damage detection to civil structures." Harbin Gongye Daxue Xuebao/Journal of Harbin Institute of Technology **40**(4): 505-513.

F. A. Diaz, E. A. P., R. A. Tomlinson, J. R. Yates (2004). "Measuring stress intensity factors during fatigue crack growth using thermoelasticity." Fatigue Fracture of Engineering Materials and Structures **27**: 571-583.

Farrar, C. R., G. Park, et al. (2006). "Sensor network paradigms for structural health monitoring." Structural Control and Health Monitoring **13**(Compendex): 210-225.

Friswell, M. I. (2002). "Crack Modeling for Structural Health Monitoring." Structural Health Monitoring **1**(2): 139-148.

Giurgiutiu, V. (2008). Structural Health Monitoring With Piezoelectric Wafer Active Sensors. London, Academic Press.

Grisso, B. L. and D. J. Inman (2006). Impedance-based structural health monitoring of thermal protection systems, Bellingham WA, WA 98227-0010, United States, International Society for Optical Engineering.

Heyman, J. S. (1990). NDE research for aging aircraft integrity. Proceedings of the IEEE 1990 Ultrasonics Symposium, December 4, 1990 - December 7, 1990, Honolulu, HI, USA, Publ by IEEE.

Inman, D. D. J. (2001). Engineering Vibration. Upper Saddle River, Prentice-Hall.

Khiem, N. T. and T. V. Lien (2001). "A simplified method for natural frequency analysis of a multiple cracked beam." Journal of Sound and Vibration **245**(4): 737-751.

Khiem, N. T. and T. V. Lien (2004). "Multi-crack detection for beam by the natural frequencies." Journal of Sound and Vibration **273**(1-2): 175-184.

Koo, K.-Y., S. Park, et al. (2007). Impedance-based structural health monitoring considering temperature effects, San Diego, CA, United States, SPIE, Bellingham WA, WA 98227-0010, United States.

Leo, D. J. (2007). Engineering Analysis of Smart Material Systems. Hoboken, John Wiley and Sons.

Liang, C., S. Fanping, et al. (1996). "Electro-mechanical impedance modeling of active material systems." Smart Materials and Structures **5**(Copyright 1996, IEE): 171-186.

Liang, C., F. P. Sun, et al. (1994). "Coupled electro-mechanical analysis of adaptive material systems-determination of the actuator power consumption and system energy transfer." Journal of Intelligent Material Systems and Structures **5**(Copyright 1994, IEE): 12-20.

Lichtenwalner, P. F., J. P. Dunne, et al. (1997). Active damage interrogation system for structural health monitoring. Smart Structures and Materials 1997: Industrial and Commercial Applications of Smart Structures Technologies, San Diego, CA, USA, SPIE.

Loutridis, S., E. Douka, et al. (2004). "Crack identification in double-cracked beams using wavelet analysis." Journal of Sound and Vibration **277**(4-5): 1025-1039.

Material, S. (2010). 2010, from http://www.smart-material.com/Smart-choice.php?from=MFC.

Mi, B., J. E. Michaels, et al. (2006). "An ultrasonic method for dynamic monitoring of fatigue crack initiation and growth." Journal of the Acoustical Society of America **119**(Compendex): 74-85.

Mitsura Egashira, N. S. (1993). "Local Strain Sensing Using Piezoelectric Polymer." Journal of Intelligent Material Systems and Structures **4**(4).

Narkis, Y. (1994). "Identification of Crack Location in Vibrating Simply Supported Beams." Journal of Sound and Vibration **172**(4): 549-558.

Pandurangan, P. and G. D. Buckner (2006). Non-destructive evaluation of metal-to-metal adhesive joints using vibration analysis: experimental results. Nondestructive Evaluation and Health Monitoring of Aerospace Materials, Composites, and Civil Infrastructure V, San Diego, CA, USA, SPIE.

Park, G., H. Sohn, et al. (2003). "Overview of piezoelectric impedance-based health monitoring and path forward." Shock and Vibration Digest **35**(6): 451-463.

Park, S., B. L. Grisso, et al. (2007). "MFC-based structural health monitoring using a miniaturized impedance measuring chip for corrosion detection." Research in Nondestructive Evaluation **18**(2): 139-150.

Pitchford, C. W. (2007). Impedance-Based Structural Health Monitoring of Wind Turbine Blades. Mechanical Engineering. Blacksburg, Virginia Tech. **Masters:** 120.

Salawu, O. S. (1997). "Detection of structural damage through changes in frequency: A review." Engineering Structures **19**(Compendex): 718-723.

Schull, P. J. (2002). Nondestructive Evaluation: Theory, Techniques, and Applications. New York, Marcel Dekker.

Shigley, J. E. M., Charles R.; Buynas, Richard G. (2004). Mechanical Engineering Design. J. R. L. Jack P. Holman. New York, McGraw-Hill.

Y. Fujimoto, G. L., Y. Tanaka, E. Im (2004). "Stress Intensity Factor Measurement of Cracks Using a Piezoelectric Element." Society for Experimental Mechanics **44**(3).

Yuhang, H. and Y. Yaowen (2007). "Wave propagation modeling of the PZT sensing region for structural health monitoring." Smart Materials and Structures **16**(Copyright 2008, The Institution of Engineering and Technology): 706-716.

Yukio Fujimoto, E. S., Gernot Pirker, Gang Liu (2003). "Piezoelectric sensor for stress intensity factor measurement of two dimensional cracks." Engineering Fracture Mechanics **70**: 1203-1218.

Yukio Fujimoto, E. S., Gernot Pirker, Yoshikazu Tanaka (2003). "Stress Intensity Factor Measurement of Two-Dimensional Cracks by the Use of Piezoelectric Sensor." JSME International Journal **46**(4).

Zhang, W. (1999). "Closure Effects on Fatigue Crack Detection." Journal of Engineering Mechanics **125**(10): 1125-1132.

Appendices:

Appendix A: Numerical Codes
Appendix B: Natural Frequency Figures

Appendix A: Numerical Codes

Mathematica Code for Calculating Natural Frequencies of cracked beams

```
Clear [all]

"Describing the Beam";

"all values in SI";

Moe = 73.1*10^9;"Pa";



L = 0.24;

base= 0.0191;

height= 0.0045;



Rho = 2780 ;
```

```
"Values necessary for Uncracked Natural Frequency and Critical Loading";

Iner= (base * ((height)^3))/12

mhat = Rho * base * height;



"Solving Critical loading and operating condition load";

Pcr= □^2 * Moe * Iner / (L^2);

P = 0.000001;
```

```
Print[Pcr]

"Solving Cracked natural Frequency"

"Describing the Crack ";

Xc = 0.015;  "Crack Location ";

ai = 0; "Crack Depth (m)";


allofit[ai_]:=(


   Kb = Moe * Iner;

   Lambda = Sqrt [ P / (2 * Kb)];

   K = (mhat * W^2 / Kb)^(1/4);



   K1 = Lambda * Sqrt [ 1 + Sqrt[ 1 + (K / Lambda)^4 ]];

   K2 = Lambda * Sqrt [ -1 + Sqrt[ 1 + (K / Lambda)^4 ]];





   r = ai/height;

   f = 1.862 * r^2 - 3.95 * r^3 + 16.375 * r^4 - 37.226 * r^5 + 76.81 * r^6 - 126 * r^7 + 172 * r^8
- 143.97 * r^9 + 66.56 * r^10;
```

```
c1 = 5.436 * height * f;


S1[x_] = (K2^2/ (K1^2 + K2^2))* Cos[K1 * x] + (K1^2/ (K1^2 + K2^2)) * Cosh[K2 * x];

S2[x_] = (K2^2 / (K1 * (K1^2 + K2^2))) * Sin[K1 * x] + (K1^2 / (K2 * (K1^2 + K2^2))) *
Sinh[ K2 * x];

S3[x_] = (-1/ (K1^2 + K2^2)) * Cos[K1 * x] + (1/ (K1^2 + K2^2)) * Cosh[K2 * x];

S4[x_] = (-1 / (K1 * (K1^2 + K2^2))) * Sin[K1 * x] + (1 / (K2 * (K1^2 + K2^2))) * Sinh[K2 *
x];


d11S1=D[S1[x],x];

d1S1[x_]=d11S1;

d11S2=D[S2[x],x];

d1S2[x_]=d11S2;

d11S3=D[S3[x],x];

d1S3[x_]=d11S3;

d11S4=D[S4[x],x];

d1S4[x_]=d11S4;


d22S1=D[d11S1, x];

d2S1[x_]=d22S1;

d22S2=D[d11S2, x];

d2S2[x_]=d22S2;

d22S3=D[d11S3, x];
```

```
d2S3[x_]=d22S3;
d22S4=D[d11S4, x];
d2S4[x_]=d22S4;

d33S1=D[D[D[S1[x],x],x],x];
d3S1[x_]=d33S1;
d33S2=D[D[D[S2[x],x],x],x];
d3S2[x_]=d33S2;
d33S3=D[D[D[S3[x],x],x],x];
d3S3[x_]=d33S3;
d33S4=D[D[D[S4[x],x],x],x];
d3S4[x_]=d33S4;



Mone = (-d2S3[L]/Kb + c1*(S2[L-Xc]-(P/Kb)*d2S4[L-Xc])*(-d2S3[Xc]/Kb));
Mtwo = (-d3S3[L]-(P/Kb)*d1S3[L]+c1*(Kb*(d3S2[L-Xc]-(P/Kb)*d3S4[L-Xc])+P*(d1S2[L-
Xc]-(P/Kb)*d1S4[L-Xc]))*(-d2S3[Xc]/Kb));
Vone = (-d2S4[L]/Kb + c1*(S2[L-Xc]-(P/Kb)*d2S4[L-Xc])(-d2S4[Xc]/Kb));
Vtwo = (-d3S4[L]-(P/Kb)*d1S4[L]+c1*(Kb*(d3S2[L-Xc]-(P/Kb)*d3S4[L-Xc])+P*(d1S2[L-
Xc]-(P/Kb)*d1S4[L-Xc]))*(-d2S4[Xc]/Kb));

Roos=(Mone*Vtwo-Mtwo*Vone);
```

```
  FindRoot[Roos==0,{W,400}]

  );
allofit[0]
allofit[height]
```

```
cracksize=Table[x, {x, 0, 0.0043, 0.0001}]

ListPlot[{cracksize, R}□]
```

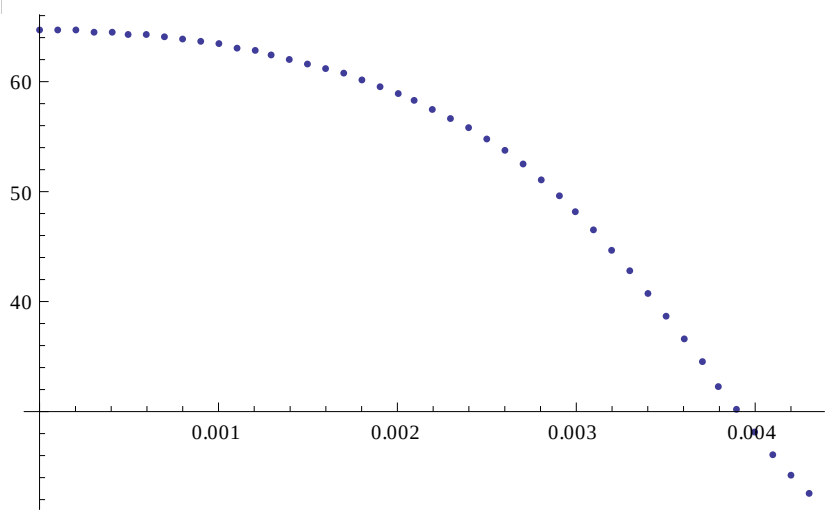

Matlab Code for Simulating Beating Due to Smallest Shift in Natural Frequency

```
[X1, temp]=Decay(4096, 100, 0.001, 65.78);
```

```
[X2, temp]=Decay(4096, 100, 0.001, 65.52);
X3=X1-X2;
figure, plot(temp, X3);
xlabel('time(sec)');
ylabel('Amplitude');
figure, plot(temp, X1);
xlabel('time(sec)');
ylabel('Amplitude');
figure, plot(temp, X2);
xlabel('time(sec)');
ylabel('Amplitude');
```

Matlab Code for Frequency Analysis of Experimental Beam Using SigLab Measurement System

```
clc
clear all
close all

%Load the data file
load baseline.vna -mat

%Extract the data.  Note that the scale factors must be set appropriately.
freq=SLm.fdxvec;
voltran1=SLm.xcmeas(1,3).xfer;%Divide by 100 because of gain on PZT coupler
veltran1=SLm.xcmeas(1,3).xfer;
coher=SLm.xcmeas(1,2).coh;
```

```
%Plot the FRF
hold on
semilogy(freq,abs(voltran1),'b')

load damagecase1.vna -mat

%Extract the data.  Note that the scale factors must be set appropriately.
freq=SLm.fdxvec;
voltran1=SLm.xcmeas(1,3).xfer*86.6/100;%Divide by 100 because of gain on PZT coupler
veltran1=SLm.xcmeas(1,3).xfer*0.025*86.6/100;
coher=SLm.xcmeas(1,2).coh;

%Plot the FRF
hold on
semilogy(freq,abs(voltran1),'b')


load damagecase2.vna -mat

freq=SLm.fdxvec;
voltran1=SLm.xcmeas(1,3).xfer*86.6/100;%Divide by 100 because of gain on PZT coupler
veltran1=SLm.xcmeas(1,3).xfer*0.025*86.6/100;%0.125 for 500, 0.025 for 100, 0.005 for 50
coher=SLm.xcmeas(1,2).coh;

%Plot the FRF
hold on
semilogy(freq,abs(voltran1),'b')
```

```
load damagecase3.vna -mat

freq=SLm.fdxvec;
voltran1=SLm.xcmeas(1,3).xfer*86.6/100;%Divide by 100 because of gain on PZT coupler
veltran1=SLm.xcmeas(1,3).xfer*0.025*86.6/100;%0.125 for 500, 0.025 for 100, 0.005 for 50
coher=SLm.xcmeas(1,2).coh;

%Plot the FRF
hold on
semilogy(freq,abs(voltran1),'b')

load damagecase4.vna -mat

freq=SLm.fdxvec;
voltran1=SLm.xcmeas(1,3).xfer*86.6/100;%Divide by 100 because of gain on PZT coupler
veltran1=SLm.xcmeas(1,3).xfer*0.025*86.6/100;
coher=SLm.xcmeas(1,2).coh;

%Plot the FRF
hold on
semilogy(freq,abs(voltran1),'b')

load damagecase5.vna -mat

freq=SLm.fdxvec;
voltran1=SLm.xcmeas(1,3).xfer*86.6/100;%Divide by 100 because of gain on PZT coupler
```

```
veltran1=SLm.xcmeas(1,3).xfer*0.025*86.6/100;
coher=SLm.xcmeas(1,2).coh;

%Plot the FRF
hold on
semilogy(freq,abs(voltran1),'b')

load damagecase6.vna -mat

freq=SLm.fdxvec;
voltran1=SLm.xcmeas(1,3).xfer*86.6/100;%Divide by 100 because of gain on PZT coupler
veltran1=SLm.xcmeas(1,3).xfer*0.025*86.6/100;
coher=SLm.xcmeas(1,2).coh;

%Plot the FRF
hold on
semilogy(freq,abs(voltran1),'b')
```

Matlab Code for Processing Time Series Data to Establish Beat Phenomena

```
clc
clear all
close all

%Load the data file
load jan27c52k.vos -mat;
decay1= SLm.scmeas(1).tdmeas;
```

```
% Plot Baseline Decay Signal
figure, plot(SLm.tdxvec, abs(decay1/max(decay1)));
xlabel('time (sec)');
ylabel('amplitude (Volts)');

% Read in Damaged Signal
load jan27c131p1k.vos -mat;
decay2= SLm.scmeas(1).tdmeas;



figure, plot(SLm.tdxvec, abs(decay2/max(decay2)));
xlabel('time (sec)');
ylabel('amplitude (Volts)');

% Establish Beats Via Subtraction
beats=decay1-decay2;

figure, plot(SLm.tdxvec, abs(beats));
xlabel('time (sec)');
ylabel('amplitude (Volts)');
xlabel('time (sec)');
ylabel('amplitude (Volts)');
% Establish Frequency Spectrum Using Fourier Transforms
frf=(2/8096)*fft(decay2, 8096);
freq=0:1:4047;
figure, plot(freq/pi, abs(frf(1:4048)))
xlabel('frequency(hz)');
```

```
ylabel('amplitude');
```

Matlab Code for Reading in Impedance Data and Calculating RMSD Damage Index

```
close all

clear all

% Read Impedance Files into Matlab

load baselineA.txt

load AFeb2c30k.txt

load AFeb2c60k.txt

load AFeb2c90k.txt

load AFeb2c120k.txt

load AFeb2c150k.txt

load AFeb2c180k.txt

load AFeb2c190k.txt

load AFeb2c193k.txt

load A2Feb2c193k.txt

load AFeb2c196k.txt

load AFeb2c198k.txt

% Build Impedance Matrix for real Impedances

imp=zeros(4000, 12);

imp(1:4000, 1)=baselineA(1:4000, 2);

imp(1:4000, 2)=AFeb2c30k(1:4000, 2);

imp(1:4000, 3)=AFeb2c60k(1:4000, 2);

imp(1:4000, 4)=AFeb2c90k(1:4000, 2);

imp(1:4000, 5)=AFeb2c120k(1:4000, 2);

imp(1:4000, 6)=AFeb2c150k(1:4000, 2);

imp(1:4000, 7)=AFeb2c180k(1:4000, 2);

imp(1:4000, 8)=AFeb2c190k(1:4000, 2);
```

```
imp(1:4000, 9)=AFeb2c193k(1:4000, 2);
imp(1:4000, 10)=A2Feb2c193k(1:4000, 2);
imp(1:4000, 11)=AFeb2c196k(1:4000, 2);
imp(1:4000, 12)=AFeb2c198k(1:4000, 2);

% Plot Impedance Spectrums
w0=baselineA(1:4000, 1);
for i=1:12;
   hold on
   plot(w0, imp(1:4000, i));
   xlabel('frequency (Hz)');
   ylabel('magnitude of real impedance');
end

%
% Calculate RMSD damage Index
RMSD=zeros(12,1);
RMSDs=zeros(12,1);
for j=1:12
  for r=1:length(w0)
    RMSD(j, 1)= RMSD(j,1) + power((imp(r, 1)-imp(r, j)), 2)/(power(imp(r,1), 2));
  end
  RMSDs(j, 1)=power(RMSD(j,1),0.5);
end
% Plot RMSD
figure
plot(RMSDs);
figure
```

```
bar(RMSDs, 1);
xlabel('damage case')
ylabel('RMSD')
figure
plot(cracklength, RMSDs);


figure
semilogy(w0, imp(1:4000, length(cracklength)), 'r')
hold on
semilogy(w0, imp(1:4000, 1))
xlabel('frequency (Hz)');
ylabel('magnitued of real impedance');
```

Matlab Code for Calculation of Stress Intensity Factors from Voltage Data and Analytical SIF

```
close all
clear all
%Input beam dimensions in millimeters (lower case)
w=25.4;
t=3.175;
l=226;
area=w*t;


%Input crack length vector stress vector and cycles vector
a=[0 0 0 0 0 0 0 0 0 0 0.5 0.5 0.6 0.7 0.8 0.8 0.9 1 1.2 1.3 1.4 1.5 1.6 1.6 1.6 1.8 1.8 1.9 1.9 2 2 2 2.1 2.1 2.1 2.2 2.4
2.5 2.6 2.6 2.6 2.6 2.8 2.9 3 3.2 3.4 3.6 3.8 3.8 4 4.2 4.5 4.8 4.9 5 5.2 5.4 5.5 5.8 6 6.2 6.4 6.5 6.6 7.4 7.5 7.8 8]+1;
```

```
cycles=[69 86 96 113 120 145 150 160 180 190 220 230 240 248 250 251 268 275 282 288 291 295 300 305 310
315 330 336 340 354 360 367 374 387 390 396 400 405 408 409 418 420 424 430 438 441 447 453 454 458 465
470 473 478 480 482 485 486 489 492 494 495 496 496.7 499 503 504.2 505.8 507];
Sigma1=51.65;

%Input Voltage Output of MFC from Experiment at given crack lengths
V1=[24.6 24.8 24.8 24.8 25 25 25.4 25.4 25.4 25.6 25.8 25.8 25.8 25.8 25.8 26 25.8 25.8 26 26 26.2 26.2 26.4 26.4
26.4 26.4 26.6 26.8 27 27 27.2 27 27 26.8 27 27 27 27.2 27 27.2 27.2 27.2 27.4 27.4 27.4 27.4 27.4 27.6 27.6 27.6
27.6 27.6 27.8 27.8 28 28 28 28.2 28 27.8 27.8 26.6 25.8 25.6 25 26 25 24.8 24.6];
V2=[24.8 24.8 24.8 25 24.8 25 25 25.2 25.2 25.2 25.4 25.4 25.4 25.4 25.6 25.6 25.6 25.8 25.8 25.8 26 26 25.8 26 26
26.2 26.2 26.4 26.6 26.8 26.6 26.6 26.8 26.6 26.8 26.8 26.8 27 26.8 26.8 26.8 27 26.8 27 27.2 27.2 27.2 27.2 27.4
27.4 27.4 27.4 27.4 27.4 27.4 27.4 27.2 27.4 27.6 27.2 27.4 27.2 26.8 27 26.8 25 24.4 24.4 24];
%
DV1=diff(V1)./diff(a);
DV2=diff(V2)./diff(a);
DV1=[0 DV1];
DV2=[0 DV2];

%Calculate Theoretical SIF
Cons=zeros(length(a), 1);
K1=zeros(length(a), 1);
for I=1:length(a)
   Cons(I)=(1.1*(1-(0.2.*(a(I)./w))))./((1-(a(I)./w)).^1.5);
   K1(I)=Cons(I).*Sigma1.*sqrt(pi.*a(I));
end
```

```
%Initialize K1 vector and enter constant values for Experimental SIF
Econs=0.002;
k=1;        %k=1 for plane stress
EK1=zeros(length(a), 1);
EK2=zeros(length(a), 1);

%Input MFC active area dimensions
H=28;
L=14;
%Input distance from crack tip parameters
H0=3;
rl=0;%distance from leading edge to left pzt edge
rr=rl+L;%distance from leading edge to right pzt edge

G1=zeros(length(a), 1);
G2=zeros(length(a), 1);

%Calculate Experimental SIF's from Voltage Output of MFC

for N=1:length(a)
   L1=a(N)-rl;
   L2=rr-a(N);
   G1(N)=dblquad(@(x,y) sqrt((sqrt(x.^2+y.^2)+x)./(pi.*(x.^2+y.^2))),0, L2, H0, H0+H);
   G2(N)=dblquad(@(x,y) sqrt((sqrt(x.^2+y.^2)-x)./(pi.*(x.^2+y.^2))),0, L2, H0, H0+H);
   EK1(N)=(V1(N)+V2(N))./(2*Econs*k.*G1(N));
   EK2(N)=(V2(N)-V1(N))./(2.*Econs.*k.*G2(N));
end
```

```
%PLOT

%Plot Theoretical and Experimental SIF vs. crack length
figure, plot(a, K1, '--');
hold on
plot(a, EK1);
xlabel('crack length (mm)');
ylabel('SIF (K1)');


plot(a, EK2, 'r');
hold on
plot(a, 0, 'r', '--');
xlabel('crack length (mm)');
ylabel('SIF (K2)');

%Make Legend for SIF Plot

% %Plot crack length vs. number of cycles
figure, plot(cycles, a);
xlabel('cycles');
ylabel('crack length(mm)');
% %
%Plot V1 and V2 versus crack length
figure, plot(a, V1);
```

```
xlabel('crack length(mm)');
ylabel('Voltage');
hold on
plot(a, V2, '--');
xlabel('crack length(mm)');
ylabel('Voltage');
%
% plot cycles vs. Voltage
figure, plot(cycles, V1);
xlabel('cycles');
ylabel('Voltage A');

figure, plot(cycles, V2);
xlabel('cycles');
ylabel('Voltage B');
% Plot Derivative of Voltage
figure, plot(a, DV1);
xlabel('crack length');
ylabel('Differential of Voltage A');

figure, plot(a, DV2);
xlabel('crack length');
ylabel('differential of Voltage B');

% Plot G Factors
figure, plot(a, G1, '--');
hold on
plot(a, G2);
```

```
xlabel('crack length');

ylabel('G1, G2');
```

Appendix B: Natural Frequency Figures for In-plane experiment

Figures A-1 to A-10: Frequency spectrums from natural frequency shift experiment (In Plane)

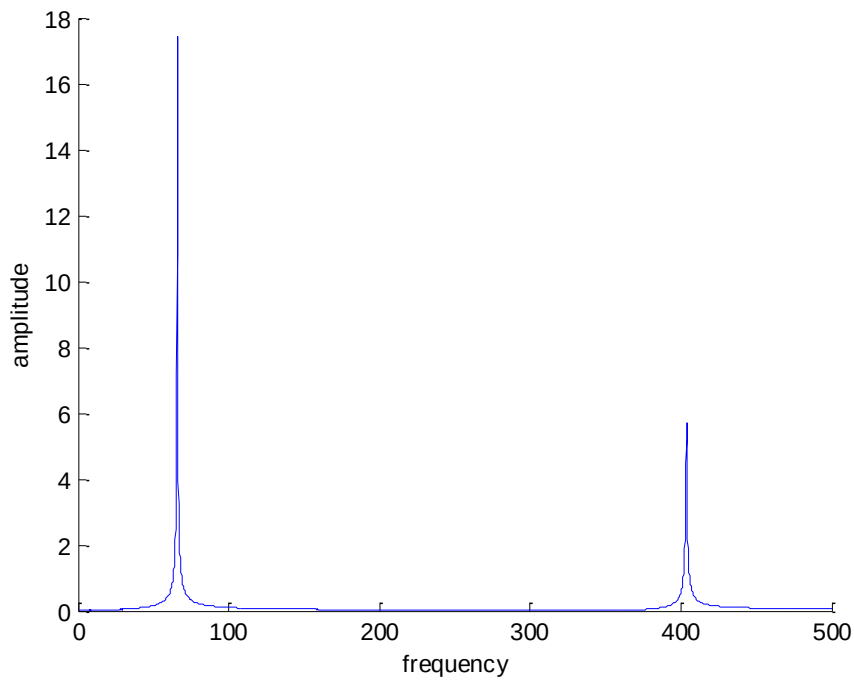

Figure A-1: Frequency response function for undamaged beam.

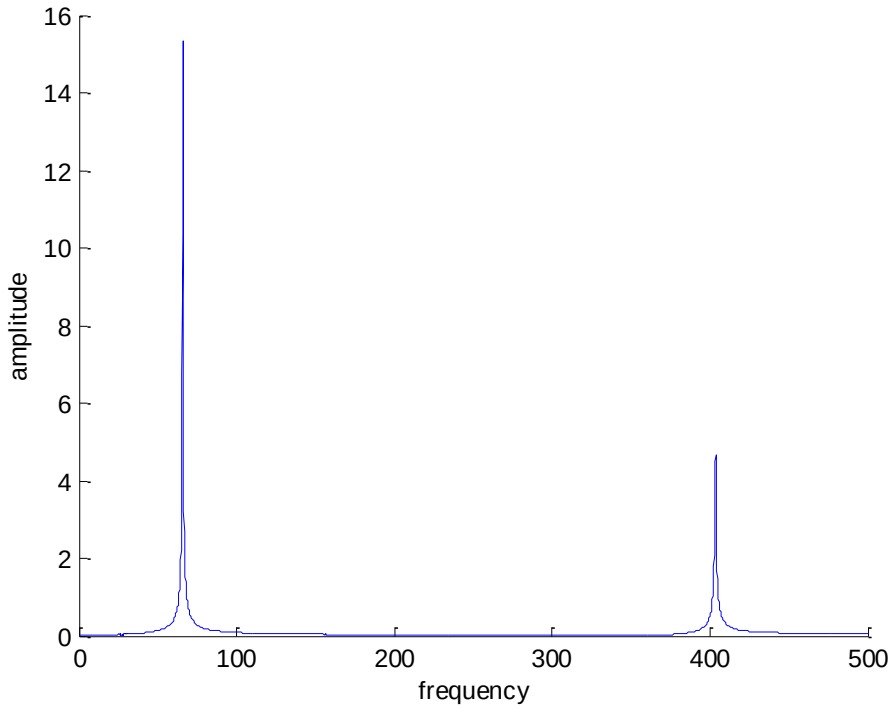

Figure A-3: Frequency response function for damage case 1.

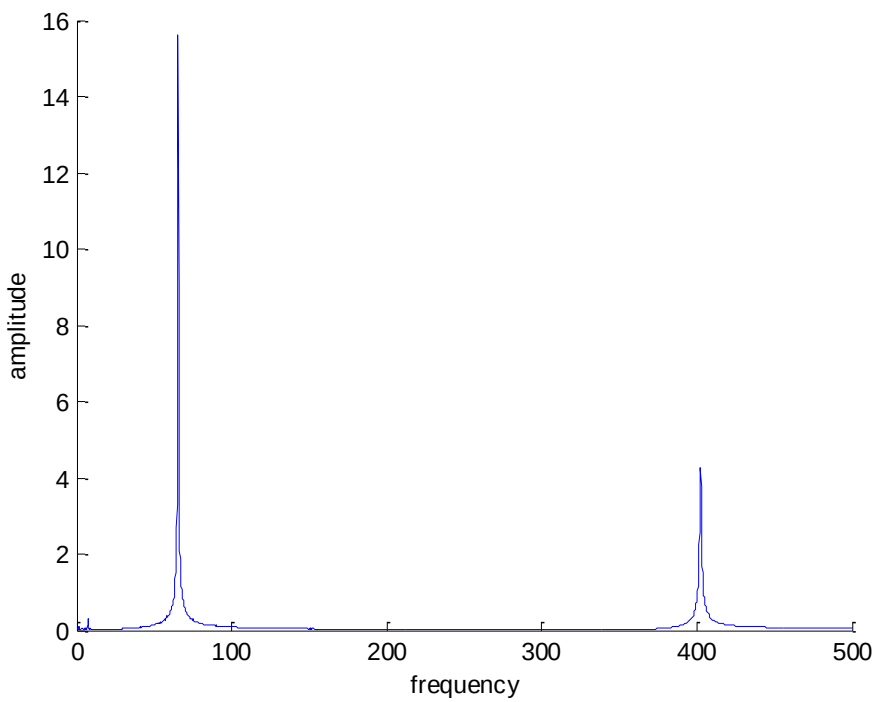

Figure A-5: Frequency response function for damage case 2.

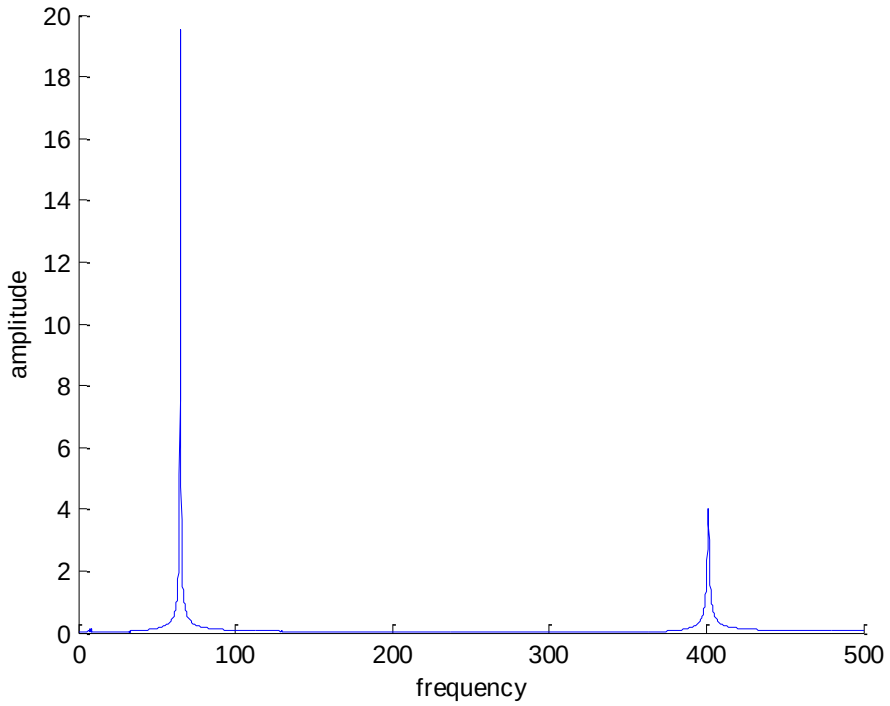

Figure A-7: Frequency response function for damage case 3.

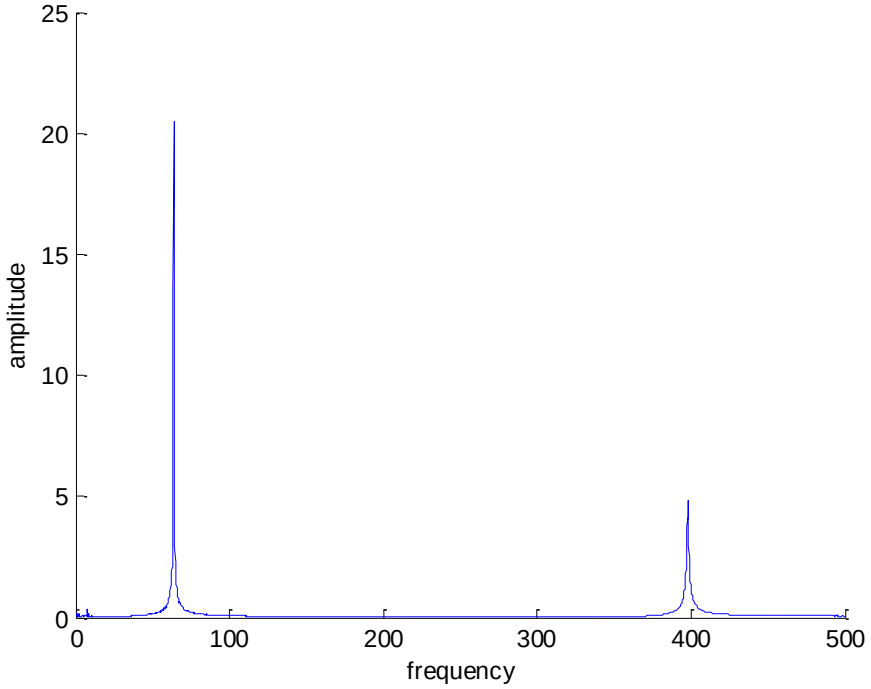

Figure A-9: Frequency response function for damage case 4.

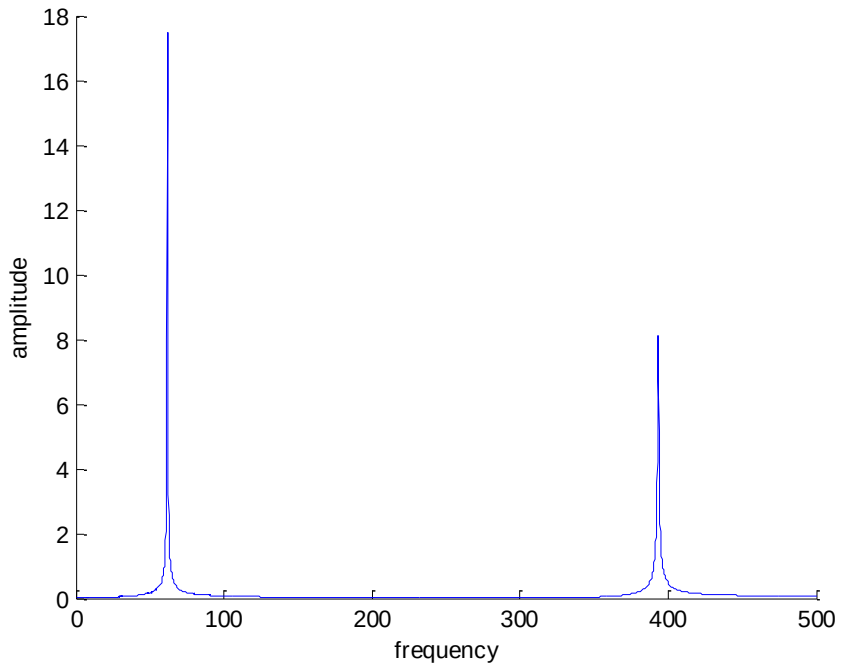

Figure A-11: Frequency response function for damage case 5.